MAGNETIC FIELD INDUCED ZINC FERRITE DISTRIBUTION IN MIXED MATRIX MEMBRANE FOR PHENOL REMOVAL

KHAIRUL ANWAR MOHAMAD SAID

A thesis submitted in fulfilment of the
requirements for the award of the degree of
Doctor of Philosophy

School of Chemical and Energy Engineering
Faculty of Engineering
Universiti Teknologi Malaysia

MARCH 2022

ACKNOWLEDGEMENT

First and foremost, I would like to express my gratitude to Almighty ALLAH for blessing me with health, strength, and inspiration along the journey for the successful completion of this PhD research. I humbly offer obeisance and salutations upon Prophet Muhammad (صلى الله عليه وسلم)the source of guidance, enlightenment, and knowledge to all mankind till the end of times. I would like to express my sincere and unfeigned appreciation to my supervisor Prof. Datuk Ts. Dr. Ahmad Fauzi Bin Ismail for encouragement, mentoring, guidance, and critics throughout my work. My profound gratitude goes to to my co-supervisor Dr. Zulhairun Bin Abdul Karim for his sincere guidance, precious time, motivation, dedication, and friendship. Without their untiring support and interest, this work would not have been the same as presented here.

I am also indebted to Universiti Malaysia Sarawak, Malaysia for providing me the resources and funding my Ph.D. study. Librarians at Universiti Teknologi Malaysia (UTM) for their assistance in providing me the relevant literatures. I would also like to wholeheartedly express my appreciation to Advanced Membrane Technology Research Centre (AMTEC), Universiti Teknologi Malaysia colleagues and all its staff for their ultimate support and inspiration.

Finally, I am extremely grateful to my beloved wife for her understanding, love, patience, dedicated late-night prayers, and support. I would like to express my deepest gratitude to my parents, without their hard work, nurturing affection and support I would not have been able to achieve anything. My sincere appreciation extends to all my colleagues and others who have provided me the assistance at various occasions. Their views and tips are useful indeed. Unfortunately, it is not possible to list all of them in this limited space.

ABSTRACT

The mixed matrix membrane typically has the particles randomly dispersed within the membrane. The random particle dispersion will reduce the adsorption and photocatalytic performance because the optimum position for particles in the membrane is near the membrane surface. At the optimum position, the particles will easily interact with the incoming targeted molecule, i.e., phenol. One of the methods to disperse the particles near the membrane is by magnetic induce casting. Hence, the first objective was to analyze the effect of magnet arrangement in magnetic induced casting on zinc ferrite distribution in the membrane for phenol adsorption. Next, was to elucidate the impact of different zinc ferrite dosage on magnetic induced casting at varied initial phenol concentrations via adsorption kinetic, isotherm, and diffusion model. The final objective was to investigate the effect of varied magnetic strength on the distribution of zinc ferrite particles in the membrane for photocatalytic degradation of phenol. The particle in this work refers to zinc ferrite, while the magnetic induced casting refers to a step during the membrane fabrication in which the cast film was exposed to magnets in different arrangements with a unique magnetic field for inducing particle distribution and migration. The membrane performance was tested by water flux, phenol adsorption, regeneration while the adsorption data were fitted into adsorption isotherm and kinetic model. For testing the hypothesis, the magnetic induced casting was carried out by arranging the magnets into the rod, circular (MB), and chain (MC) pattern while the zinc ferrite composition was varied at 3, 12 and 30 wt%. The distance between the magnet and cast film was varied to 10, 15 and 40 mm to study the influence of magnetic strength. The findings show that magnet arranged in a chain and circular pattern produced a membrane with high phenol adsorption, fast water flux and stable performance after three regeneration cycle. Circular/12wt% ZnFe (MB12) membrane reported 30.4 $L/m^2.h$ water flux with a phenol adsorption capacity of 415 mg phenol/g ZnFe (mg/g). Meanwhile, the finding shows that membrane with 3 wt%/total solid has a stable performance compared to other compositions of zinc ferrite. In studying the effect of zinc ferrite composition, the magnetic arrangement was fixed to a MC and MB pattern. Circular/3wt% ZnFe (MB3) membrane possessed a balanced water flux and phenol adsorption performance with both registering ~27 $L/m^2.h$ and ~303 mg/g, respectively. The adsorption kinetic model revealed that the diffusion in the MB3 membrane was propelled by intraparticle diffusion due to low external mass transfer coefficient, Ks = 0.000633, while the chain/3wt% ZnFe (MC3) membrane was rate-limited by external diffusion with K_s of 0.00254. The zinc ferrite adsorption stage implied that the MB3 membrane possessed a zone IV: drastic kinetic, the fastest adsorption rate, while the MC3 membrane exhibited zone III: quick kinetic, a moderate adsorption rate. Furthermore, varying the distance between magnetic and cast film revealed that the circular/12wt% ZnFe/15mm gap (MB1215) membrane demonstrated the highest photocatalytic performance with a stable photodegradation after three regeneration cycles at 1736, 1706, and 1693 mg/g phenol degradation capacity per cycle. A prolonged photocatalytic run indicated the MB1215 degraded ~98% phenol after 510 min.

ABSTRAK

Membran matriks campuran yang biasa selalunya mempunyai zarah yang diselerakkan secara rawak dalam membran. Penyebaran zarah secara rawak akan mengurangkan prestasi penjerapan dan fotopemangkinan kerana lokasi optimum bagi zarah di dalam membran ialah berdekatan dengan permukaan membran. Pada posisi optimum, zarah-zarah mudah untuk berinteraksi dengan molekul sasaran yang masuk seperti fenol. Salah satu cara untuk menyebarkan zarah hampir dengan permukaan membran ialah dengan menggunakan pencanai dorongan magnet. Oleh itu, objektif pertama ialah menganalisa kesan susunan magnet semasa mencanai dorongan magnet ke atas penyebaran zink ferit di dalam membran untuk penjerapan fenol. Seterusnya, mengkaji kesan dos zink ferit ke atas pencanai dorongan magnet pada pelbagai kepekatan fenol melalui model penjerapan isoterma dan kinetik. Objektif terakhir ialah menyiasat kesan pelbagai kekuatan magnet ke atas sebaran zarah zink ferit di dalam membran bagi fotopemangkinan fenol. Zarah dalam kajian ini merujuk kepada zink ferit sementara pencanai dorongan magnet merujuk kepada langkah semasa fabrikasi membran di mana acuan filem didedahkan pada set magnet dalam susunan yang berbeza yang mempunyai medan magnet yang unik bagi mendorong penyebaran dan penghijrahan zarah. Prestasi membran diuji dengan fluks air, penjerapan fenol, penjanaan semula sementara data penjerapan diisi ke dalam model penjerapan isoterma dan kinetik. Bagi menguji hipotesis, canaian dorongan magnet telah dilakukan dengan menyusun magnet kepada corak batang, bulatan (MB) dan rantai (MC) sementara komposisi zink ferit dipelbagaikan kepada 3, 12 and 30 wt%. Jarak diantara magnet dan filem membran dipelbagaikan kepada 10, 15 dan 40 mm bagi mengkaji kesan kekuatan magnet. Penemuan menunjukkan magnet yang di susun dengan corak rantai dan bulatan menghasilkan membran dengan penjerapan fenol tinggi, fluks air laju dan prestasi stabil setelah tiga kitaran penjanaan semula. Membran bulatan/12wt% ZnFe (MB12) melaporkan 30.4 $L/m^2.h$ fluks air dengan 415 mg fenol/g zink ferit (mg/g) kapasiti penjerapan fenol. Sementara itu, penemuan menunjukkan membran dengan 3 wt%/jumlah pepejal menunjukkan prestasi stabil berbanding komposisi zink ferit yang lain. Semasa mengkaji kesan komposisi zink ferit, susunan magnet ditetapkan pada MC dan MB. Membran bulatan/3wt% ZnFe (MB3) memiliki fluks air dan prestasi penjerapan fenol yang seimbang dengan keduanya masing- masing mendaftarkan ~27 $L/m^2.h$ and ~303 mg/g. Model penjerapan kinetik mendedahkan peresapan pada membran MB3 didorong oleh peresapan intrazarah kerana kadar pekali pemindahan jisim luaran, K_s = 0.000633 yang rendah, sementara membran rantai/3wt% ZnFe (MC3) dihadkan oleh peresapan luaran dengan K_s bersamaan 0.00254. Tahap penjerapan zink ferit menunjukkan membran MB3 memiliki zon IV:kinetik drastik, kadar penjerapan tertinggi sementara membran MC3 mempamerkan zon III:kinetik cepat, kadar penjerapan sederhana. Tambahan lagi, mempelbagai jarak antara magnet dan acuan filem mendedahkan membran bulatan/12wt% ZnFe/15mm jarak (MB1215) menunjukkan prestasi fotopemangkinan yang tinggi dengan penyusutan foto yang stabil selepas tiga kitaran penjanaan semula pada 1736, 1706, dan 1693 mg/g pada setiap kali kitaran penjanaan semula. Pemanjangan tempoh fotopemangkinan menunjukkan membran MB1215 merendahkan 98% fenol selepas 510 min.

TABLE OF CONTENTS

LIST OF TABLES

LIST OF FIGURES

LIST OF ABBREVIATIONS

AFM	-	Atomic Force Microscopy
ATR	-	attenuated total reflectance
BET	-	Brunauer, Emmett, and Teller
BJH	-	Barrett, Joyner, and Halenda
BQ	-	P-benzoquinone
BSA	-	Bovine serum albumin
CA	-	Contact angle
CLSM	-	Confocal laser scanning microscope
D-R	-	Dubinin-Radushkevich
EDX	-	Energy Dispersive X-ray
FCM	-	Iron oxide/graphitic carbon nitride
FFT	-	Fast Fourier transform
FRR	-	Fouling recovery rate
FTIR	-	Fourier Transform InfraRed spectroscopy
FWHM	-	full width half maximum
HPLC	-	High performance liquid chromatography
HRTEM	-	High-resolution transmission electron microscopy
ICDD	-	International Centre for Diffraction Data
IFFT	-	Inverse fast Fourier transform
IGO	-	Iron oxide/graphene oxide
IPA	-	Isopropanol
IRF	-	Irreversible fouling
M&W	-	Mathews and Weber model
MB	-	Magnetic induce casting circular pattern
MC	-	Magnetic induce casting chain pattern
MO	-	Mixed order model
M-O	-	Metal to oxide
MR	-	Magnetic induce casting rod pattern
NIPS	-	Nonsolvent Induced Phase Separation Process
NIR	-	Near infrared

NMP	-	N-methyl-2-pyrrolidone
NPRI	-	National Pollutant Release Inventory
OGCN	-	Oxygenated carbon nitride
PES	-	Polyethersulfone
PFO	-	Pseudo-first order model
PMR	-	Photocatalytic membrane reactor
PSO	-	Pseudo-second order model
PVP	-	Polyvinylpyrrolidone
RF	-	Reversible fouling
RhB	-	Rhodamine B
RMSE	-	Root mean square error
RO	-	Reverse osmosis
R-P	-	Redlich-Peterson
SEM	-	Scanning Electron Microscopy
SI	-	Scatter index
SMM	-	Surface modifying macromolecules
TEM	-	Transmission Electron Microscopy
TEOA	-	Triethanolamine
TF	-	Total fouling
TOC	-	Total organic compound
UK	-	United Kingdom
USA	-	United States of America
USEPA	-	US Environmental Protection Agency
UV	-	Ultraviolet
UV-Vis	-	UltraViolet-Visible spectroscopy
W&M	-	Weber and Morris model
wt%	-	Weight percentage
XPS	-	X-ray Photoelectron Spectroscopy
XRD	-	X-Ray Diffractometer
ZnFe	-	Zinc Ferrite

LIST OF SYMBOLS

$\nabla.B$	-	Field gradient of magnetic flux
B	-	Magnetic flux density
χ_c^2	-	Chi-squared test
$N_{\exp}$	-	Number of data
q_{cal}	-	Calculated data
$q_{\exp}$	-	Experimented data
C_0 / β	-	Root ratio
$K_L \beta$	-	Limiting factor
$\theta_{e1} / \theta_{e2}$	-	Ratio between adsorbate to adsorbent capacity
$\Delta\lambda$	-	Compton shift
$-\Delta G$	-	Membrane-to-liquid interfacial energy
ΔP	-	Transmembrane pressure
Δr_o	-	Film thickness, Boundary thickness
μ	-	Magnetic permeability
μ_0	-	Air permeability
^{o}	-	Degree angle
^oC	-	Degree Celsius
A	-	Effective membrane area
A	-	Fraction light in solid
B	-	Flux density
$B(\theta)$	-	Surface blocking parameter
c	-	Speed of light
C_{de}	-	Desorption concentration at equilibrium
C_e	-	Concentration at equilibrium
C_f	-	Final concentration
C_o	-	Initial concentration
CS	-	Solubility of adsorbates

C_t	-	Concentration at time, t
D^l	-	Film diffusion constant
d_p	-	Particle diameter
E	-	mean free energy
f	-	Light frequency
F_d	-	Drag force
F_m	-	Magnetic force
g	-	Exponent
H	-	Magnetic field strength
h	-	Planck's constant
h/m_0c	-	Compton wavelength
hv	-	Photon energy
I	-	Intensity
I(z)	-	Intensity at distance z below the surface
I_0	-	Surface intensity
J_{BSA}	-	BSA flux
J_{w1}	-	Membrane water flux before BSA fouling
J_{w2}	-	Membrane water flux after BSA fouling
K	-	partition coefficient
K1	-	Pseudo-first-order rate constant
K1'	-	First-order rate constant of the mixed-order model (h−1)
K2	-	Pseudo-second-order rate constant
K2'	-	Second-order rate constant of the mixed-order model
Ka	-	Adsorption constant
$k_{aadsorption}$ and $k_{desorption}$	-	rate constant
KBET1	-	Adsorption equilibrium parameters in first layer
KBET2	-	Adsorption equilibrium parameters in upper layers
KDR	-	Dubinin-Radushkevich constant
K_F	-	Freundlich constant
K_L	-	Langmuir constant
$K_{M\&W}S$	-	Intraparticle diffusion coefficient Mathews and Weber model
KRP	-	Redlich-Peterson constant

K_s	-	External mass transfer coefficient
k^{th}	-	Largest pore filled by condensation
$K_{W\&M}$	-	Mass transfer coefficient Weber & Moris model
l	-	Membrane thickness
L	-	Crystallite size
L_c	-	Crystallite size
L_g	-	Geometric path
L_s	-	Shortest path
m_p	-	Particle mass
N	-	Pore density, Number of particle per adsorption site
n	-	Number of adsorption site Ritchie equation, Number of photon
n_s	-	Amount of adsorption site Sips model
Q	-	Membrane volume flowrate
qe	-	Phenol adsorption capacity
qe_{max}	-	Maximum degradation capacity
q_{max}	-	Maximum adsorption capacity
qmBET	-	Maximum monolayer adsorbed amount
qmDR	-	Maximum adsorbed amount Dubinin-Radushkevich model
q_t	-	Adsorption at a time, t
r	-	Relative surface area
R	-	Phenol rejection, Rate constant Boyd external diffusion model, Universal gas constant
R^2	-	Coefficient of determination
$r_{adsorption}$ and $r_{desorption}$	-	the rate of adsorption and desorption
R_c		cake resistance
R_L	-	Separation factor
r_m	-	Mean pore radius
R_m		hydraulic resistance
r_o	-	Particle size
r_p		membrane pore radius
r^{th}	-	Largest pore available

S	-	Adsorbent surface area
S_a	-	Mean height
S_p	-	Maximum peak height
Sr_p	-	Strouhal number
S_v	-	Maximum valley height
S_z	-	Maximum height
t	-	Time
$t^{0.5}$	-	Square root of time
t_{ref}	-	Total period of the adsorption process
u_f	-	Fluid velocity
v	-	Particle velocity
V	-	Particle volume
V_m	-	Scalar of magnetic potential
W_{dry}	-	Dry weight
W_{wet}	-	Wet weight
z	-	Penetration depth
α	-	Significance level, Absorption coefficient
β_D	-	Full width half maximum
γ_{water}	-	Surface tension of water
δ		cake thickness
ε	-	Membrane porosity, Strain, Adsorption potential
η	-	Dynamic viscosity
θ	-	Average contact angle, Surface concentration of adsorbed particles, Scattering angle
θ_0	-	Surface coverage
θ_e	-	Surface concentration at equilibrium
θ_{e1}	-	Surface coverage fraction
θ_{e1} and θ_{e2}	-	Root solution
θ_{e2}	-	Inverted adsorption efficiency
κ	-	Shape factor, Distribution constant, Optical characteristic
λ	-	X-ray wavelength
ρ_d	-	Particle density
ρ_f	-	Fluid density

τ	-	Tortuosity
τ_A	-	External forces that push the particle at velocity A
τ_B	-	Distance for a particle with radius (r) cover through Brownian motion
τ_g	-	Geometric tortuosity
χ	-	Susceptibility
χd^2	-	Approximated chi-squared
χm	-	Medium susceptibility

LIST OF APPENDICES

CHAPTER 1

INTRODUCTION

1.1 Research Background

Membrane comes in various types: mixed matrix, thin-film, hollow fiber, nanofiber, and ceramic membrane [1,2]. Although membranes come in different shapes, the function is similar for selective removal. A mixed matrix membrane has a unique structure, divided into either symmetric or asymmetric [3]. Meanwhile, the mixed matrix term refers to the particle being immobilized in the membrane [4]. Thus, a mixed matrix membrane with an asymmetric structure is a membrane that has a distinct dense and porous layer. The thin layer is usually has a dense structure with a finger-like structure. A thin layer in the mixed matrix membrane act as the sieving filter that performs selective removal. Meanwhile, the support layer in the mixed matrix membrane typically presents a porous structure with apparent macrovoids formed throughout the layer—the support layer functions as the pillar that holds the thin layer together [5].

Although membrane with its current form would sieve the targeted particle or molecules from the feed solution, particle inclusion within its matrix could introduce a new ability or improve the existing function. Some functions other than sieving that could be offered through particle immobilization are adsorption and photocatalysis [6,7]. Adsorption involves the attachment of a targeted molecule or particle onto the adsorption site of an adsorbent either through physisorption or chemisorption [8]. In general, most of the adsorption that occurs on an immobilized adsorbent takes place through physisorption. Therefore, when the feed solution permeated the membrane, the large molecule or particle would be sieved through its small pores by the thin membrane layer. However, the molecules or particles smaller than the membrane pore radius would permeate. Hence, the adsorbent is introduced to absorb the small particles without modifying the pore radius to remedy the situation.

Meanwhile, as the name suggests, photocatalysis is a process associated with a catalyst activated by light [9]. Although photocatalysis is usually performed by suspending the catalyst in the raw solution, the method required tedious catalyst recovery at the end of the photocatalysis process [10]. Therefore, incorporating photocatalyst into the membrane eliminates the extra step to recover the catalyst. Besides, a membrane with a photocatalyst would perform two functions simultaneously; sieving and photocatalysis [11].

In normal circumstances, for a mixed matrix membrane, the immobilized particles are randomly distributed, and homogenous particle distribution is ideal for a mixed matrix membrane [4]. Although homogenous particle distribution would benefit the membrane from particle aggregation and consistent membrane performance, the selective removal feature of the immobilized particles such as adsorption and photocatalysis would be affected by the homogenous distribution. The systematic particle migration and distribution would give the mixed matrix membrane a massive advantage, mainly used for adsorption and photocatalysis application.

The primary sources of phenol and its derivatives presence in the environment are through landfill untreated leachate, municipal sewage, and industrial effluent. Even at low concentrations, the presence of phenol is known to develop cancerous cells, and it has been classified as toxic when released to the environment [12]. So far, the probable cause of phenol leaching into the water ecosystem is due to poor waste management. Therefore, several stages of water treatment must be introduced to clean the water from phenol and its derivatives before being discharged, such as introducing a membrane technology at the polishing stages. It has been categorized under priority pollutants by the US Environmental Protection Agency (USEPA) and Canada through the National Pollutant Release Inventory (NPRI) [13]. Even the international regulatory bodies have set a strict limit of phenol discharge to the environment, i.e., USEPA has imposed a strict water purity standard where phenol concentration in water surface must be lower than 1 ppb [14]. However, human and animal toxicity level to phenol exposure was as high as 9−25 mg/l [15]. The strict rule regarding phenol discharge was due to its high reactivity, meaning phenol was susceptible to interact or react with other compounds present in the water. Membrane technologies are a reliable

method to separate phenol, and it has several advantages such as small footprint, moderate power consumption depending on the pressure requirement with stable effluent quality, and easy to scale up to treat higher feed flow rate. The drawback of any membrane was fouling, mostly when particles and colloids were deposited on the membrane. Several membrane configurations focus on removing phenol from wastewater, such as hollow fiber membrane, membrane bioreactor, photocatalytic membrane, high-pressure membranes such as nanofiltration and reverse osmosis. So, to combat membrane fouling and, at the same time, utilize it as support for catalysts, the researcher has introduced a photocatalytic membrane [16]. The generated reactive oxygen species (ROS) resulting from photocatalysis reaction would assist in degrading the pollutant presence in feed solution and mitigate the formation of the fouling cake layer on the membrane surface. The addition of photocatalyst by immobilization would minimize fouling rate, reduce cleaning frequency, and stabilized pumping rate.

A photocatalyst requires access to light for activation. The light harnessing catalyst will perform its full potential when the photon energy from the light can excite an electron for a photocatalytic reaction to occur [17]. Typically, a photocatalysis process is carried out by suspending the catalyst in a sample solution [18]. Therefore, when the light was irradiated inside or directly toward the sample solution, the catalyst will easily harness the light to start the photocatalytic reaction. Although suspended photocatalysis can efficiently perform the photocatalytic reaction, an extra step is needed to recover the catalyst at the end of the process. Hence, by immobilizing the catalyst inside a membrane, the extra step for recovering the catalyst can be omitted. A photocatalytic membrane will have two functions operated simultaneously, sieving by the membrane pore and photocatalysis degradation. The particle positioned within the membrane will dictate the performance of the photocatalytic reaction due to light availability [19].

Another argument that implies the importance of dispersing the catalyst near the membrane surface is the light penetration depth. The light penetration depth is a phenomenon of light penetrating the solid surface [20]. Unlike translucent material such as glass, the polymer membrane usually restrict light from penetrating its structure. Hence, based on the Beer-Lambert law, the light penetration depth can be

estimated by the inverse of the absorption coefficient [20,21]. Although the light can penetrate a solid up to a certain distance, Beer-Lamber law dictates that the light intensity will reduce farther the light travels from the point of entry [22]. Besides reducing light intensity, the light, which, according to Arthur H. Compton, comprises photons, would experience a loss in photon energy when colliding with an electron [23]. The transfer of photon energy onto the electron of the catalyst will excite the electron of the catalyst, thus initiate a photocatalytic reaction [24,25]. Thus, both factors will directly affect the performance of photocatalyst in producing electrons required for photocatalytic reaction. By accommodating all factors, a catalyst positioned near the membrane surface surmount the random particle distribution and benefits photocatalysis in the long term.

1.2 Problem Statement

The particle position in the membrane influences its effectiveness when encountered with the targeted molecules [26]. Hence, several methods have been developed to address this issue by coating the particle on the membrane surface through interfacial polymerization, dip-coating, and vapor deposition [27–29]. Although coating the membrane would position the particle strategically, the coating would interfere with the membrane pore by blocking or shrinking the pore radius and affect the membrane [30]. Moreover, the coated particle was prone to leaching and coating delamination [31]. Therefore, for an ideal mixed matrix membrane, the immobilized particles should be beneath the membrane surface to simulate the coating technique.

It is challenging to manipulate the particles in a homogeneously mixed polymer solution during membrane fabrication. However, in recent years, particle manipulation has been accomplished by external forces such as magnetic fields or with chemical assistance [19,26]. For particle manipulation via chemical pathways, the particle migration within the membrane is accomplished by phase inversion [26]. During phase inversion, the additive would diffuse out along with the solvent into the non-solvent, which migrated the particle within the cast film to the membrane surface. Although

the chemical approach has successfully migrated the particles, the controlled manipulation relies upon additive and homogeneity in the dope solution, influencing its repeatability.

In contrast, particle manipulation through a magnetic field would produce a consistent migration and distribution [32]. The major drawback of magnetic field-assisted particle manipulation is that it only applies to magnetically attracted particles such as metal. Besides the limitation, the magnetic field would be a perfect method to induce particle migration and distribution with endless configuration. In recent years, magnetic induce casting for membrane fabrication has been applied in many areas of membrane technology, such as reverse osmosis, nanofiltration, ultrafiltration, fuel cell, and photocatalysis [33–36]. However, the application of magnets during membrane fabrication is limited to hovering the magnet parallel to the cast film. Although the approach will migrate the particles, the particle distribution depends on the magnetic field lines [37]. The magnetic field lines of a permanent magnet are based upon the magnet shape. For instance, a bar magnet will produce different magnetic lines compared to a horseshoe shape magnet.

Moreover, another factor influencing particle manipulation by a magnet was its magnetic force strength [38]. The intensity of the magnetic force would determine the distribution of particles across the membrane matrix, and a strong magnetic attraction force could eventually pull out the particle from the cast film. Hence, at an ideal condition, the magnetic force strength would sufficiently distribute the particles and migrated them without causing the particles to leap out of the cast film and stick on the permanent magnet. For a mixed matrix membrane with adsorption characteristics, the adsorbent order in its matrix would determine the effectiveness of the overall membrane efficacy in adsorbing the targeted material. Hence, by dispersing the adsorbent as close as possible to the membrane surface, the travel time before adsorbate interacts with the adsorbent can be reduced, thus increasing the probability of adsorption. In contrast, if the adsorbents were randomly distributed throughout the membrane, the time taken before the adsorbent interacts with the adsorbate would increase, which simultaneously lower the probability of adsorption.

Therefore, it is justifiable to disperse the particle to be as close as possible to the membrane surface. Besides, the particle positioned inside the membrane matrix would be less prone to leaching, thus allowing for regeneration and prolonged application. Figure 1.1 illustrates the effect of the particle positioned within the membrane on its adsorption performance. Hence, an optimum position for catalyst immobilized in a photocatalytic membrane is close to the membrane surface, similar to an adsorptive membrane. Based on this inference, the magnetic induce approach is better suited for migrating and distributing the particle than the chemical-assisted particle manipulation. Albeit chemical-assisted particle manipulation will cause a similar outcome to the magnetic induce method, i.e., particle manipulation, the inclusion of chemicals in a dope solution will cause an unwanted reaction with the catalyst. Therefore, the photocatalytic membrane would benefit more by magnetic induce particle manipulation to avoid unnecessary reactions to the catalyst.

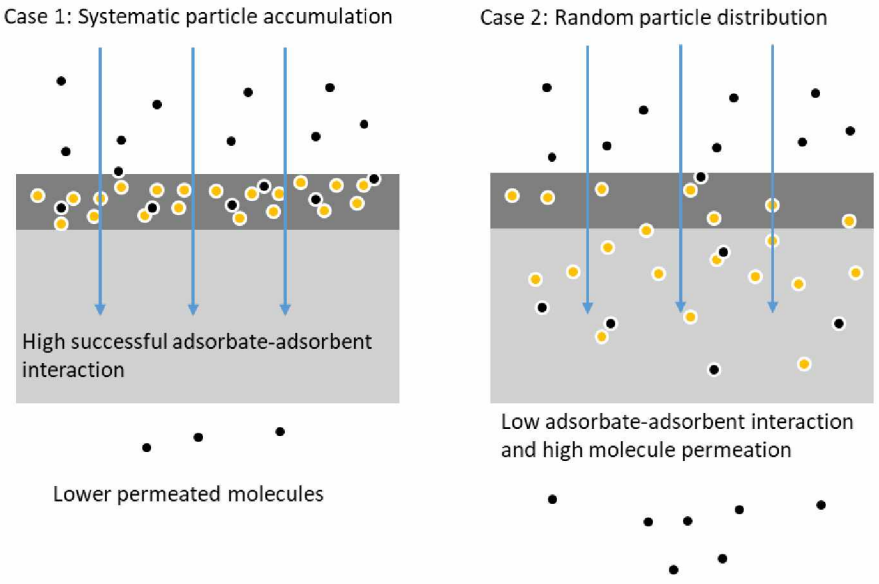

Figure 1.1 Schematic diagram illustrating the effect of particle distribution on adsorption. Case 1: systematic particle accumulation near the membrane surface and Case 2: random particle distribution in the membrane.

Figure 1.2 illustrates the effect of light penetration depth on catalyst immobilized in a membrane. A suitable particle for magnetic induce casting must be magnetically attracted metal such as ferrite-based materials. Zinc ferrite possesses such properties, and besides being attracted to a magnet, it is also capable of adsorbing

and degrading organic pollutants such as phenol [39,40]. Therefore, by incorporating zinc ferrite in a mixed matrix membrane and with the assistance of magnetic induce casting, it is possible to disperse zinc ferrite near the membrane surface. A mixed matrix membrane that consists of a systematically dispersed zinc ferrite would perform efficiently to adsorb the permeating phenol. Meanwhile, exposure to a light source would transform the mixed matrix membrane from an adsorptive membrane to a photocatalytic membrane. Zinc ferrite would make a suitable particle for a magnetic induce casting prepared mixed matrix membrane capable of adsorption and photodegrading phenol for water treatment. An optimum mixed matrix membrane to be considered in water treatment would possess a good sieving ability with added functionalities such as adsorption and photocatalysis, which could be obtained by dispersing the particle inside the membrane near its surface.

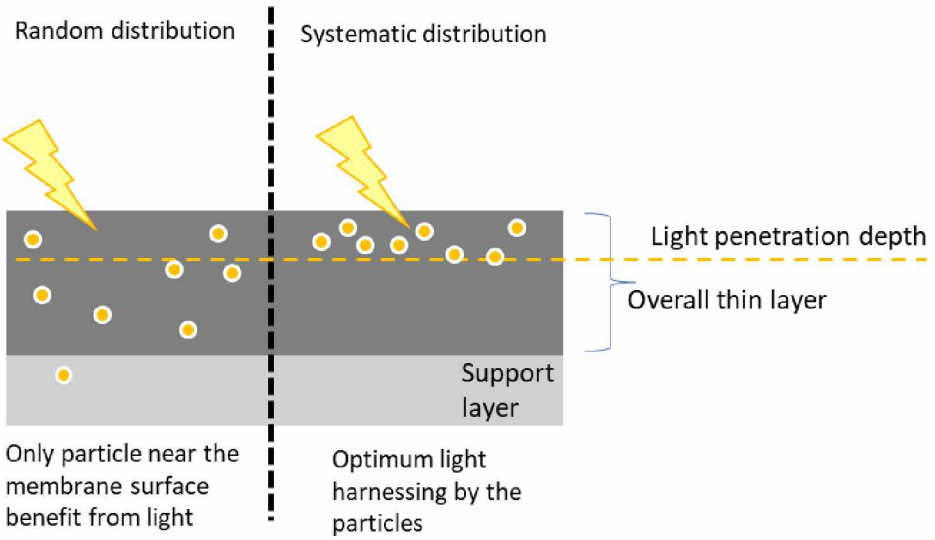

Figure 1.2 The benefit of particle accumulating close to membrane surface in a photocatalytic membrane.

In order to investigate the influence of particle dispersion by the magnetic field, a set of objectives was devised to investigate the effectiveness of systematic particle dispersion on adsorption and photocatalytic membrane. The magnets are arranged in a pattern resulting in a unique magnetic field to assist in zinc ferrite dispersion. Besides arranging the magnets, the magnetic strength was also varied to observe its effect on zinc ferrite dispersion. Therefore, the novelty of this work lies in utilizing magnets in terms of pattern and strength to induce particle dispersion.

1.3 Research Objectives

Based on the problems mentioned earlier, the following objectives are formulated to explore the systematic particle migration and distribution in the membrane via magnetic field:

(a) To analyze the effect of magnet arrangement in magnetic induce casting on zinc ferrite distribution in the membrane for phenol adsorption;

(b) To elucidate the impact of different zinc ferrite dosage on magnetic induce casting at varied initial phenol concentrations via adsorption kinetic, isotherm, and diffusion model;

(c) To investigate the effect of varied magnetic strength on the distribution of zinc ferrite particles in the membrane for photocatalytic degradation of phenol

1.4 Research Scopes

The following research scopes presented a parameter boundary when examining each objective for a detailed and in-depth study:

Objective 1:

(a) Zinc ferrite was synthesized according to the co-precipitation method with zinc nitrate hexahydrate ($Zn(NO_3)_3 \cdot 6H_2O$, $\geq$ 99% crystallized) and iron nitrate nonahydrate ($Fe(NO_3)_3 \cdot 9H_2O$, $\geq$ 99.999% trace metals basis) supplied by Sigma Aldrich as the precursor. The zinc ferrite composition is fixed at 12 wt% and calculated based on per total solid basis. The total solid refers to the composition of polyethersulfone (PES, $C_{12}H_8O_3S$, Radel A300, Ameco Performance) that makes up the membrane. The polyethersulfone composition was fixed at 18 wt%. Therefore, the zinc ferrite composition was 12 wt% from the overall weight of PES. Polyvinylpyrrolidone (PVP, $(C_6H_9NO)n$, K30,

Sigma Aldrich) 1 wt% was added to assist pore formation and weighed based on a per total solution basis. The total solution refers to the total composition of the dope solution, which comprises a polymer and solvent. The solvent was 82 wt% N-methyl-2-pyrrolidone (NMP, C_5H_9NO, V-Chem). The membrane was fabricated by a non-solvent induced phase separation process (NIPS) method with water as the non-solvent.

(b) The permanent magnet used to achieve the objective was 60 button-shaped magnets (200 mT/each, Neodynium, One Magnet) arrangement in a circular, chain, and rod pattern. The magnet in the particular pattern was suspended above the cast film at a fixed distance of 40 mm. For circular patterns, each loop contains 6 button magnets with 9 loops fixed across a steel plate. For the chain pattern, 12 button magnets were bound side-by-side to form 5 lines of chain pattern fixed next to each other on a steel plate. Meanwhile, the rod pattern magnet was arranged by binding the button magnet surface-to-surface, creating a long magnet rod with 60 button magnets. For the rod pattern, the magnetic induce casting was conducted by placing the rod in a hollow glass tube. The glass tube was used to spread the membrane across the glass plate, and with a rod pattern, the magnetic rod was moved along with the glass tube, creating direct magnetic exposure onto the cast film. Unlike rod patterns, the other two patterns would be conducted by suspending the magnet above the cast film.

(c) The membrane was characterized by scanning electron microscopy (SEM), energy dispersive X-ray (EDX), atomic force microscopy (AFM), Fourier transform infrared spectroscopy (FTIR), a gravimetric method for porosity measurement, contact angle analysis, water flux test at 1 bar, and zeta potential.

(d) The phenol adsorption was conducted by the dead-end filtration method. Phenol initial concentration was fixed at 30 ppm, with a total volume of 1 liter per adsorption test, and the adsorption interval was standardized at 120 min. All adsorption test was conducted at room temperature (26-28 °C). The adsorption data were fitted to several adsorption isotherms categorized as chemical adsorption, physical adsorption, Polanyi potential adsorption, and

empirical adsorption. Ultraviolet-visible spectrometry (UV-vis) analyzed the permeated solution at 270 nm wavelength.

(e) The membrane regeneration was conducted in three cycles with sodium chloride.

(f) Two magnetic arrangements that produce the best performance membrane will be chosen for studying objective 2.

Objective 2:

(a) The membrane fabrication condition was similar to scope (a) of objective 1, with changes to zinc ferrite composition. The composition was varied for 3, 12, and 30 wt% per total solid basis.

(b) The magnetic pattern was limited to circular and chain patterns. The magnetic induce casting procedure was similar to the scope (b) of objective 1.

(c) The initial phenol concentration was varied, starting from 5, 13, and 30 ppm. The adsorption test was conducted on dead-end filtration for 120 min at 1 bar, and data were fitted into the adsorption kinetic models. The kinetic model was categorized into adsorption reaction, external and internal diffusion, and adsorption onto active sites. UV-vis was used to analyze the permeated solution at 270 nm wavelength.

(d) Membrane characterization was similar to the scope (c) of objective 1.

(e) Membrane regeneration was similar to the scope (e) of objective 1.

(f) The zinc ferrite loading that produces the best performance membrane and magnetic arrangement from scope (e) of objective 1 will be used to study objective 3.

Objective 3:

(a) The zinc ferrite composition was fixed at 12 wt% while the magnetic pattern was circular and chain pattern with membrane fabrication similar to scope (a) and (b) of objective 1.

(b) The magnetic strength was varied by manipulating the distance between magnet and cast film. The distances were 10, 15, and 40 mm, and in term of the magnetic field were 150, 70, and 10 mT measured by portable Gauss meter (WT103 digital Tesla meter, China).

(c) The photocatalysis was conducted with UV light (254 nm) for 330 min while for stability test, the photocatalytic interval increased to 550 min. The adsorption period was fixed at 30 min before photocatalysis begins. The photocatalysis setup was conducted via submerged flat sheet membrane. High-performance liquid chromatography (HPLC) was used to analyze the membrane permeate. Initial phenol concentration was standardized at 5 ppm for a total volume of 0.9 L and solution regulated to pH 5. The amount of catalyst in the membrane was calculated based on 12 wt% of membrane mass and applicable for determining the adsorbed phenol at equilibrium (q_e).

(d) The adsorption kinetics and isotherm model was conducted according to the scope (d) of objective 1 and scope (c) of objective 2.

(e) Membrane regeneration was conducted similar to the scope (e) of objective 1.

(f) Membrane fouling was carried out via protein sieving. The model protein was bovine serum albumin (BSA, Sigma Aldrich), and initial concentration was regulated to 1,000 ppm for a total volume of 1 L. The fouling test was conducted by dead-end filtration, and membrane permeate was analyzed by UV-vis at 280 nm wavelength. Membrane regeneration for fouling test implemented by soaking in water.

1.5 Significance of the study

This study explored the possibility of achieving systematic particle arrangement within the membrane matrix. The membrane was exposed to a series of magnetic patterns that induce the particle migration and assist its distribution across the membrane surface. Hence, from this study, the significance findings would be a membrane that possesses particles aligned close to the membrane surface, exhibiting higher adsorption and photocatalysis performance. Therefore, this study would offer an alternative view of the influence of particle distribution on the existing concept of a mixed matrix membrane. The alternative view would be the particles distributed upwards towards the membrane surface were preferable to the former concept that suggests homogenous particle distribution throughout the mixed matrix membrane. From membrane fabrication perspective, the magnetic induce casting would be the most straightforward and cost-effective approach for attaining a membrane with consistent particle distribution.

1.6 Thesis outline

This thesis is structured in seven chapters, mainly zinc ferrite synthesis and membrane fabrication by various magnetic patterns and strength with different zinc ferrite compositions. The membrane was tested on phenol adsorption and phenol mineralization by photocatalysis. Chapter 1 emphasizes the problem statement, which is the motivation of this work. From the problem statement, a set of objectives were formulated to address the problem. The research scopes were proposed to achieve the objectives and provide a perimeter around the objective.

Chapter 2 introduced the current mixed matrix membrane, followed by particle manipulation. The particle dispersion is divided into chemical, and magnetic force approaches. A review of the current chemical and magnetic approach for particle dispersion was presented, which revealed a research gap worth exploring. Next, an alternative view was presented, which features the importance of a mixed matrix membrane in which the particle was systematically aligned near the membrane surface

instead of randomly scattered within the membrane matrix. Then, a theory was presented to highlight the light penetration on solid surfaces, such as membrane and photon-electron collision relationships, showing the significance of systematic particle distribution in the photocatalytic membrane.

Chapter 3 presents the methodology of particle synthesis, membrane fabrication, adsorption study, fitting of adsorption data to kinetic and isotherm model, membrane regeneration, fouling studies, and photocatalysis.

Chapter 4 explains the effect of various magnetic patterns on particle dispersion on phenol adsorption. The adsorption mechanism was proposed by fitting the adsorption data into several isotherm models.

Chapter 5 report the effect of different zinc ferrite composition on particle dispersion under different magnetic pattern exposure. The findings in this chapter revealed the optimum zinc ferrite composition for magnetic induce casting. The effect of zinc ferrite composition was evaluated by phenol adsorption at various initial concentrations. The adsorption data were fitted in several kinetic models to assert a mechanism of phenol adsorption.

Chapter 6 explore the impact of magnetic strength on particle migration and distribution within the membrane in which the membrane was fitted in a submerged membrane module for photocatalytic degradation of phenol. The magnetic strength shows that ordered particle dispersion is a significant factor in improving the photocatalysis process.

Chapter 7 concludes each chapter in result and discussion and suggests recommendations to extend the present study.

REFERENCES

1. Abitha, V. K., Thomas, S. Fabrication Methods: Polymer Membranes for Liquid Transport. Transport Properties of Polymeric Membranes. Elsevier; 2017. 35–50 p.
2. Qiu, M., Chen, X., Fan, Y., Xing, W. Ceramic Membranes. In: Drioli E, Giorno L, Fontananova EBT-CMS and E (Second E, editors. Comprehensive Membrane Science and Engineering Oxford: Elsevier; 2017. p. 270–97.
3. Jiang, L. Y. Asymmetric Membrane BT - Encyclopedia of Membranes. In: Drioli E, Giorno L, editors. Berlin, Heidelberg: Springer Berlin Heidelberg; 2016. p. 126–7.
4. Donato, L., Garofalo, A., Algieri, C. 3 - Mixed-matrix membranes: Preparation and characterization for biorefining. In: Figoli A, Cassano A, Basile ABT-MT for B, editors. Woodhead Publishing; 2016. p. 61–84.
5. Robeson, L. M. Polymer Membranes. In: Matyjaszewski K, Möller MBT-PSACR, editors. Polymer Science: A Comprehensive Reference Amsterdam: Elsevier; 2012. p. 325–47.
6. Wu, H., Inaba, T., Wang, Z.-M., Endo, T. Photocatalytic TiO2@CS-embedded cellulose nanofiber mixed matrix membrane. *Appl. Catal. B Environ.*, 2020. 276: 119111.
7. Shahrin, S., Lau, W.-J., Goh, P.-S., Ismail, A. F., Jaafar, J. Adsorptive mixed matrix membrane incorporating graphene oxide-manganese ferrite (GMF) hybrid nanomaterial for efficient As(V) ions removal. *Compos. Part B Eng.*, 2019. 175: 107150.
8. Berger, A. H., Bhown, A. S. Comparing physisorption and chemisorption solid sorbents for use separating CO2 from flue gas using temperature swing adsorption. *Energy Procedia*, 2011. 4: 562–7.
9. Koe, W. S., Lee, J. W., Chong, W. C., Pang, Y. L., Sim, L. C. An overview of photocatalytic degradation: photocatalysts, mechanisms, and development of photocatalytic membrane. *Environ. Sci. Pollut. Res.*, 2020. 27(3): 2522–65.

10. Vaiano, V., Iervolino, G. Facile method to immobilize ZnO particles on glass spheres for the photocatalytic treatment of tannery wastewater. *J. Colloid Interface Sci.*, 2018. 518: 192–9.
11. Pereira, V. R., Isloor, A. M., Bhat, U. K., Ismail, A. F., Obaid, A., Fun, H.-K. Preparation and performance studies of polysulfone-sulfated nano-titania (S-TiO 2) nanofiltration membranes for dye removal. *RSC Adv.*, 2015. 5(66): 53874–85.
12. Hori, T. S. F., Avilez, I. M., Inoue, L. K., Moraes, G. Metabolical changes induced by chronic phenol exposure in matrinxã Brycon cephalus (teleostei: characidae) juveniles. *Comp. Biochem. Physiol. Part C Toxicol. Pharmacol.*, 2006. 143(1): 67–72.
13. Villegas, L. G. C., Mashhadi, N., Chen, M., Mukherjee, D., Taylor, K. E., Biswas, N. A Short Review of Techniques for Phenol Removal from Wastewater. *Curr. Pollut. Reports*, 2016. 2(3): 157–67.
14. Sun, X., Wang, C., Li, Y., Wang, W., Wei, J. Treatment of phenolic wastewater by combined UF and NF/RO processes. *Desalination*, 2015. 355: 68–74.
15. Sunil, K., Jayant, K. Review on Research for Removal of Phenol from Wastewater. *Int. J. Sci. Res. Publ.*, 2013. 3(4): 1–5.
16. Dzinun, H., Othman, M. H. D., Ismail, A. F. Photocatalytic performance of TiO2/Clinoptilolite: Comparison study in suspension and hybrid photocatalytic membrane reactor. *Chemosphere*, 2019. 228: 241–8.
17. Lee, K. M., Lai, C. W., Ngai, K. S., Juan, J. C. Recent developments of zinc oxide based photocatalyst in water treatment technology: A review. *Water Res.*, 2016. 88: 428–48.
18. Ng, K. H., Chen, K., Cheng, C. K., Vo, D.-V. N. Elimination of energy-consuming mechanical stirring: Development of auto-suspending ZnO-based photocatalyst for organic wastewater treatment. *J. Hazard. Mater.*, 2020. : 124532.
19. Li, B., Meng, M., Cui, Y., Wu, Y., Zhang, Y., Dong, H., Zhu, Z., Feng, Y., Wu, C. Changing conventional blending photocatalytic membranes (BPMs): Focus on improving photocatalytic performance of Fe3O4/g-C3N4/PVDF membranes through magnetically induced freezing casting method. *Chem. Eng. J.*, 2019. 365: 405–14.

20. Douplik, A., Saiko, G., Schelkanova, I., Tuchin, V. V. 3 - The response of tissue to laser light. In: Jelínková HBT-L for MA, editor. Woodhead Publishing Series in Electronic and Optical Materials Woodhead Publishing; 2013. p. 47–109.

21. Sidorov, I. S., Miridonov, S. V., Nippolainen, E., Kamshilin, A. A. Estimation of light penetration depth in turbid media using laser speckles. *Opt. Express*, 2012. 20(13): 13692.

22. Ash, C., Dubec, M., Donne, K., Bashford, T. Effect of wavelength and beam width on penetration in light-tissue interaction using computational methods. *Lasers Med. Sci.*, 2017. 32(8): 1909–18.

23. Compton, A. H. A Quantum Theory of the Scattering of X-rays by Light Elements. *Phys. Rev.*, 1923. 21(5): 483–502.

24. Moreira, J. Photocatalytic Degradation of Phenolic Compounds in Water: Irradiation and Kinetic Modelling. 2011. (August): 217.

25. Hussein, E. M. A. CHAPTER ONE - MECHANISMS. In: Hussein EMABT-RM, editor. Oxford: Elsevier Science Ltd; 2007. p. 1–65.

26. Salim, N. E., Nor, N. A. M., Jaafar, J., Ismail, A. F., Qtaishat, M. R., Matsuura, T., Othman, M. H. D., Rahman, M. A., Aziz, F., Yusof, N. Effects of hydrophilic surface macromolecule modifier loading on PES/O-g-C3N4 hybrid photocatalytic membrane for phenol removal. *Appl. Surf. Sci.*, 2019. 465(May 2018): 180–91.

27. Mavukkandy, M. O., McBride, S. A., Warsinger, D. M., Dizge, N., Hasan, S. W., Arafat, H. A. Thin film deposition techniques for polymeric membranes–A review. *J. Memb. Sci.*, 2020. 610: 118258.

28. Xia, L., Vemuri, B., Saptoka, S., Shrestha, N., Chilkoor, G., Kilduff, J., Gadhamshetty, V. Chapter 1.8 - Antifouling Membranes for Bioelectrochemistry Applications. In: Mohan SV, Varjani S, Pandey ABT-MET, editors. Biomass, Biofuels and Biochemicals Elsevier; 2019. p. 195–224.

29. Huang, C.-Y., Ko, C.-C., Chen, L.-H., Huang, C.-T., Tung, K.-L., Liao, Y.-C. A simple coating method to prepare superhydrophobic layers on ceramic alumina for vacuum membrane distillation. *Sep. Purif. Technol.*, 2018. 198: 79–86.

30. Grosso, D. How to exploit the full potential of the dip-coating process to better control film formation. *J. Mater. Chem.*, 2011. 21(43): 17033–8.

31. Li, X.-M., Ji, Y., Yin, Y., Zhang, Y.-Y., Wang, Y., He, T. Origin of delamination/adhesion in polyetherimide/polysulfone co-cast membranes. *J. Memb. Sci.*, 2010. 352(1): 173–9.

32. Zinadini, S., Zinatizadeh, A. A. L., Rahimi, M., Vatanpour, V. Magnetic field-augmented coagulation bath during phase inversion for preparation of ZnFe2O4/SiO2/PES nanofiltration membrane: A novel method for flux enhancement and fouling resistance. *J. Ind. Eng. Chem.*, 2017. 46: 9–18.

33. Huang, Z. Q., Chen, Z. Y., Guo, X. P., Zhang, Z., Guo, C. L. Structures and separation properties of PAN-Fe3O4 ultrafiltration membranes prepared under an orthogonal magnetic field. *Ind. Eng. Chem. Res.*, 2006. 45(23): 7905–12.

34. Huang, Z. Q., Zheng, F., Zhang, Z., Xu, H. T., Zhou, K. M. The performance of the PVDF-Fe 3O 4 ultrafiltration membrane and the effect of a parallel magnetic field used during the membrane formation. *Desalination*, 2012. 292: 64–72.

35. Zhao, Z., Hu, J., Zhou, Z., Zhong, M. The use of Strong Magnetic Field Treatment for Preparation of Proton Exchange Membrane Doped by SeO2 and its electrochemical properties. *Int. J. Electrochem. Sci.*, 2017. 12(6): 5450 – 5463.

36. Hu, Xa., Sun, J., Peng, R., Tang, Q., Luo, Y., Yu, P. Novel thin-film composite reverse osmosis membrane with superior water flux using parallel magnetic field induced magnetic multi-walled carbon nanotubes. *J. Clean. Prod.*, 2020. 242: 118423.

37. Ido, Y., Yamaguchi, T., Kiuchi, Y. Distribution of micrometer-size particles in magnetic fluids in the presence of steady uniform magnetic field. *J. Magn. Magn. Mater.*, 2011. 323(10): 1283–7.

38. Zhang, Y., Gao, J., Yasuda, H., Kolbe, M., Wilde, G. Particle size distribution and composition in phase-separated Cu75Co25 alloys under various magnetic fields. *Scr. Mater.*, 2014. 82: 5–8.

39. Kefeni, K. K., Mamba, B. B. Photocatalytic application of spinel ferrite nanoparticles and nanocomposites in wastewater treatment: Review. *Sustain. Mater. Technol.*, 2020. 23: e00140.

40. Dehghani, F., Hashemian, S., Shibani, A. Effect of calcination temperature for capability of MFe2O4 (M = Co, Ni and Zn) ferrite spinel for adsorption of bromophenol red. *J. Ind. Eng. Chem.*, 2017. 48: 36–42.

41. Davidson, R. S. The photodegradation of some naturally occurring polymers. *J. Photochem. Photobiol. B Biol.*, 1996. 33(1): 3–25.

42. Tsuruta, Y., Watanabe, S., Inoue, H. Fluorometric Determination of Phenol andp-Cresol in Urine by Precolumn High-Performance Liquid Chromatography Using 4-(N-Phthalimidinyl)benzenesulfonyl Chloride. *Anal. Biochem.*, 1996. 243(1): 86–91.

43. Max, B., Tugores, F., Cortés-Diéguez, S., Domínguez, J. M. Bioprocess Design for the Microbial Production of Natural Phenolic Compounds by Debaryomyces hansenii. *Appl. Biochem. Biotechnol.*, 2012. 168(8): 2268–84.

44. Ghasemzadeh, A., Jaafar, H. Z. E., Rahmat, A. Synthesis of Phenolics and Flavonoids in Ginger (Zingiber officinale Roscoe) and Their Effects on Photosynthesis Rate. Vol. 11, International Journal of Molecular Sciences . 2010.

45. Phan, C. T., Letouze, R. A comparative study of chlorophyll, phenolic and protein contents, and of hydroxycinnamate:CoA ligase activity of normal and 'vitreous' plants (Prunus avium L.) obtained in vitro. *Plant Sci. Lett.*, 1983. 31(2): 323–7.

46. Montgomery-Brown, J., Reinhard, M. Occurrence and Behavior of Alkylphenol Polyethoxylates in the Environment. *Environ. Eng. Sci.*, 2003. 20(5): 471–86.

47. Kohler, H.-P. E., Gabriel, F. L. P., Giger, W. <I>ipso</I>-Substitution – A Novel Pathway for Microbial Metabolism of Endocrine-Disrupting 4-Nonylphenols, 4-Alkoxyphenols, and Bisphenol A. *Chim. Int. J. Chem.*, 2008. 62(5): 358–63.

48. Patnaik, P., Khoury, J. N. Reaction of phenol with nitrite ion: pathways of formation of nitrophenols in environmental waters. *Water Res.*, 2004. 38(1): 206–10.

49. Vione, D., Maurino, V., Minero, C., Pelizzetti, E. Phenol photonitration upon UV irradiation of nitrite in aqueous solution I: Effects of oxygen and 2-propanol. *Chemosphere*, 2001. 45(6): 893–902.

50. Moussavi, M. Effect of polar substituents on autoxidation of phenols. *Water Res.*, 1979. 13(12): 1125–8.

51. Kinney, L. C. Photolysis Mechanisms for Pollution Abatement. Federal Water Pollution Control Administartion; 1969. (Advanced waste treatment research laboratory).

52. Huyskens, P., Mullens, J., Gomez, A., Tack, J. Solubility of Alcohols, Phenols and Anilines in Water. *Bull. des Sociétés Chim. Belges*, 1975. 84(3): 253–62.

53. McCall, I. C., Betanzos, A., Weber, D. A., Nava, P., Miller, G. W., Parkos, C. A. Effects of phenol on barrier function of a human intestinal epithelial cell line correlate with altered tight junction protein localization. *Toxicol. Appl. Pharmacol.*, 2009/08/11. 2009. 241(1): 61–70.

54. Schweigert, N., Zehnder, A. J. B., Eggen, R. I. L. Chemical properties of catechols and their molecular modes of toxic action in cells, from microorganisms to mammals. *Environ. Microbiol.*, 2001. 3(2): 81–91.

55. Anku, W. W., Mamo, M. A., Govender, P. P. Phenolic Compounds in Water: Sources, Reactivity, Toxicity and Treatment Methods. In: Phenolic Compounds - Natural Sources, Importance and Applications InTech; 2017. p. 13.

56. Munoz-de-Toro, M., Markey, C., Wadia, P. R., Luque, E. H., Rubin, B. S., Sonnenschein, C., Soto, A. M. Perinatal exposure to Bisphenol A alters peripubertal mammary gland development in mice. *Endocrinology*, 2005. 146(9): 4138–47.

57. vom Saal, F. S., Hughes, C. An extensive new literature concerning low-dose effects of bisphenol A shows the need for a new risk assessment. *Environ. Health Perspect.*, 2005. 113(8): 926–33.

58. Saha, N. C., Bhunia, F., Kaviraj, A. Toxicity of phenol to fish and aquatic ecosystems. *Bull. Environ. Contam. Toxicol.*, 1999. 63(2): 195–202.

59. Jin, X., Zha, J., Xu, Y., Giesy, J. P., Wang, Z. Toxicity of pentachlorophenol to native aquatic species in the Yangtze River. *Environ. Sci. Pollut. Res.*, 2012. 19(3): 609–18.

60. Orton, F., Lutz, I., Kloas, W., Routledge, E. J. Endocrine Disrupting Effects of Herbicides and Pentachlorophenol: In Vitro and in Vivo Evidence. *Environ. Sci. Technol.*, 2009. 43(6): 2144–50.

61. Li, E., Bolser, D. G., Kroll, K. J., Brockmeier, E. K., Falciani, F., Denslow, N. D. Comparative toxicity of three phenolic compounds on the embryo of fathead minnow, Pimephales promelas. *Aquat. Toxicol.*, 2018. 201: 66–72.

62. Livingston, A. G. A novel membrane bioreactor for detoxifying industrial wastewater: I. Biodegradation of phenol in a synthetically concocted wastewater. *Biotechnol. Bioeng.*, 1993. 41(10): 915–26.

63. Ren, L.-F., Chen, R., Zhang, X., Shao, J., He, Y. Phenol biodegradation and microbial community dynamics in extractive membrane bioreactor (EMBR) for phenol-laden saline wastewater. *Bioresour. Technol.*, 2017. 244: 1121–8.

64. Pimple, S., Karikkat, S., Devanna, M., Yanamadni, V., Sah, R., Prasad, S. M. R. Comparison of MBR/RO and UF/RO hybrid systems for the treatment of coke-oven effluents. *Desalin. Water Treat.*, 2016. 57(7): 3002–10.

65. Al-Obaidi, M. A., Jarullah, A. T., Kara-Zaïtri, C., Mujtaba, I. M. Simulation of hybrid trickle bed reactor–reverse osmosis process for the removal of phenol from wastewater. *Comput. Chem. Eng.*, 2018. 113: 264–73.

66. Al-Obaidi, M. A., Kara-Zaïtri, C., Mujtaba, I. M. Removal of phenol from wastewater using spiral-wound reverse osmosis process: Model development based on experiment and simulation. *J. Water Process Eng.*, 2017. 18: 20–8.

67. Ji, Y., Qian, W., Yu, Y., An, Q., Liu, L., Zhou, Y., Gao, C. Recent developments in nanofiltration membranes based on nanomaterials. *Chinese J. Chem. Eng.*, 2017. 25(11): 1639–52.

68. Ochando-Pulido, J. M., Corpas-Martínez, J. R., Martinez-Ferez, A. About two-phase olive oil washing wastewater simultaneous phenols recovery and treatment by nanofiltration. *Process Saf. Environ. Prot.*, 2018. 114: 159–68.

69. Chen, S.-H., Yu, K.-C., Lin, S.-S., Chang, D.-J., Liou, R. M. Pervaporation separation of water/ethanol mixture by sulfonated polysulfone membrane. *J. Memb. Sci.*, 2001. 183(1): 29–36.

70. Jian, K., Pintauro, P. N. Asymmetric PVDF hollow-fiber membranes for organic/water pervaporation separations. *J. Memb. Sci.*, 1997. 135(1): 41–53.

71. Cao, S., Shi, Y., Chen, G. Influence of acetylation degree of cellulose acetate on pervaporation properties for MeOH/MTBE mixture. *J. Memb. Sci.*, 2000. 165(1): 89–97.

72. Li, D., Yao, J., Sun, H., Liu, B., van Agtmaal, S., Feng, C. Recycling of phenol from aqueous solutions by pervaporation with ZSM-5/PDMS/PVDF hollow fiber composite membrane. *Appl. Surf. Sci.*, 2018. 427: 288–97.

73. Rawindran, H., Lim, J.-W., Goh, P.-S., Subramaniam, M. N., Ismail, A. F., Radi bin Nik M Daud, N. M., Rezaei-Dasht Arzhandi, M. Simultaneous separation and degradation of surfactants laden in produced water using PVDF/TiO2 photocatalytic membrane. *J. Clean. Prod.*, 2019. 221: 490–501.

74. Algamdi, M. S., Alsohaimi, I. H., Lawler, J., Ali, H. M., Aldawsari, A. M., Hassan, H. M. A. Fabrication of graphene oxide incorporated polyethersulfone hybrid ultrafiltration membranes for humic acid removal. *Sep. Purif. Technol.*, 2019. 223: 17–23.

75. Zhou, K.-G., McManus, D., Prestat, E., Zhong, X., Shin, Y., Zhang, H.-L., Haigh, S. J., Casiraghi, C. Self-catalytic membrane photo-reactor made of carbon nitride nanosheets. *J. Mater. Chem. A*, 2016. 4(30): 11666–71.

76. Melcher, J., Barth, N., Schilde, C., Kwade, A., Bahnemann, D. Influence of TiO2 agglomerate and aggregate sizes on photocatalytic activity. *J. Mater. Sci.*, 2017. 52(2): 1047–56.

77. Wetchakun, K., Wetchakun, N., Sakulsermsuk, S. An overview of solar/visible light-driven heterogeneous photocatalysis for water purification: TiO2- and ZnO-based photocatalysts used in suspension photoreactors. *J. Ind. Eng. Chem.*, 2019. 71: 19–49.

78. Santoro, D., Crapulli, F., Turolla, A., Antonelli, M. Detailed modeling of oxalic acid degradation by UV-TiO2 nanoparticles: Importance of light scattering and photoreactor scale-up. *Water Res.*, 2017. 121: 361–73.

79. Oblak, R., Kete, M., Štangar, U. L., Tasbihi, M. Alternative support materials for titania photocatalyst towards degradation of organic pollutants. *J. Water Process Eng.*, 2018. 23: 142–50.

80. Mohammadi, Z., Sharifnia, S., Shavisi, Y. Photocatalytic degradation of aqueous ammonia by using TiO2ZnO/LECA hybrid photocatalyst. *Mater. Chem. Phys.*, 2016. 184: 110–7.

81. Mozia, S. Photocatalytic membrane reactors (PMRs) in water and wastewater treatment. A review. *Sep. Purif. Technol.*, 2010. 73(2): 71–91.

82. Alhaji, M. H., Sanaullah, K., Khan, A., Hamza, A., Muhammad, A., Ishola, M. S., Rigit, A. R. H., Bhawani, S. A. Recent developments in immobilizing

titanium dioxide on supports for degradation of organic pollutants in wastewater- A review. *Int. J. Environ. Sci. Technol.*, 2017. 14(9): 2039–52.

83. Liu, T., Wang, L., Liu, X., Sun, C., Lv, Y., Miao, R., Wang, X. Dynamic photocatalytic membrane coated with ZnIn2S4 for enhanced photocatalytic performance and antifouling property. *Chem. Eng. J.*, 2020. 379: 122379.

84. Bellardita, M., Camera-Roda, G., Loddo, V., Parrino, F., Palmisano, L. Coupling of membrane and photocatalytic technologies for selective formation of high added value chemicals. *Catal. Today*, 2020. 340: 128–44.

85. Chin, M. L., Mohamed, A. R., Bhatia, S. Photodegradation of Methylene Blue Dye in Aqueous Stream Using Immobilized TiO2 Film Catalyst: Synthesis, Characterization and Activity Studies. *J. Teknol.*, 2012. .

86. Zheng, X., Shen, Z.-P., Shi, L., Cheng, R., Yuan, D.-H. Photocatalytic Membrane Reactors (PMRs) in Water Treatment: Configurations and Influencing Factors. Vol. 7, Catalysts . 2017.

87. Riaz, S., Park, S.-J. An overview of TiO2-based photocatalytic membrane reactors for water and wastewater treatments. *J. Ind. Eng. Chem.*, 2020. 84: 23–41.

88. Kumakiri, I., Diplas, S., Simon, C., Nowak, P. Photocatalytic Membrane Contactors for Water Treatment. *Ind. Eng. Chem. Res.*, 2011. 50(10): 6000–8.

89. Pirola, C., Bianchi, C. L., Gatto, S., Ardizzone, S., Cappelletti, G. Pressurized photo-reactor for the degradation of the scarcely biodegradable DPC cationic surfactant in water. *Chem. Eng. J.*, 2013. 225: 416–22.

90. Chin, S. S., Chiang, K., Fane, A. G. The stability of polymeric membranes in a TiO2 photocatalysis process. *J. Memb. Sci.*, 2006. 275(1): 202–11.

91. Drioli, E., Fontananova, E. Catalytic Membranes Embedding Selective Catalysts: Preparation and Applications. In: Barbaro P, Liguori F, editors. Heterogenized Homogeneous Catalysts for Fine Chemicals Production: Materials and Processes Dordrecht: Springer Netherlands; 2010. p. 203–29.

92. Koe, W. S., Lee, J. W., Chong, W. C., Pang, Y. L., Sim, L. C. An overview of photocatalytic degradation: photocatalysts, mechanisms, and development of photocatalytic membrane. *Environ. Sci. Pollut. Res.*, 2020. 27(3): 2522–65.

93. Yeh, T.-F., Cihlář, J., Chang, C.-Y., Cheng, C., Teng, H. Roles of graphene oxide in photocatalytic water splitting. *Mater. Today*, 2013. 16(3): 78–84.

94. Salazar, H., Martins, P. M., Santos, B., Fernandes, M. M., Reizabal, A., Sebastián, V., Botelho, G., Tavares, C. J., Vilas-Vilela, J. L., Lanceros-Mendez, S. Photocatalytic and antimicrobial multifunctional nanocomposite membranes for emerging pollutants water treatment applications. *Chemosphere*, 2020. 250: 126299.

95. Cittrarasu, V., Balasubramanian, B., Kaliannan, D., Park, S., Maluventhan, V., Kaul, T., Liu, W. C., Arumugam, M. Biological mediated Ag nanoparticles from Barleria longiflora for antimicrobial activity and photocatalytic degradation using methylene blue. *Artif. Cells, Nanomedicine, Biotechnol.*, 2019. 47(1): 2424–30.

96. Mohamad Said, K. A., Ismail, A. F., Karim, Z. A., Abdullah, M. S., Hafeez, A., Azali, M. A. Magnetic rod induced asymmetric membrane: Effect of iron oxide composition to phenol removal by adsorption. *Mater. Chem. Phys.*, 2021. 258(April 2020): 123862.

97. Wu, H., Lin, Y., Wu, J., Zeng, L., Zeng, D., Du, J. Surface Adsorption of Iron Oxide Minerals for Phenol and Dissolved Organic Matter. *Earth Sci. Front.*, 2008. 15(6): 133–41.

98. Mulder, M. Basic Principles of Membrane Technology. Springer; 1996.

99. Mishra, S., Yadav, S. S., Rawat, S., Singh, J., Koduru, J. R. Corn husk derived magnetized activated carbon for the removal of phenol and para-nitrophenol from aqueous solution: Interaction mechanism, insights on adsorbent characteristics, and isothermal, kinetic and thermodynamic properties. *J. Environ. Manage.*, 2019. 246(April): 362–73.

100. Wang, J., Guo, X. Adsorption kinetic models: Physical meanings, applications, and solving methods. *J. Hazard. Mater.*, 2020. 390(November 2019): 122156.

101. Boyd, G. E., Adamson, A. W., Myers, L. S. The Exchange Adsorption of Ions from Aqueous Solutions by Organic Zeolites. II. Kinetics 1. *J. Am. Chem. Soc.*, 1947. 69(11): 2836–48.

102. Mathews, A. P., Weber Jr., W. J. Effects of external mass transfer and intraparticle diffusion on adsorption rates in slurry reactors. *AIChE Symp. Ser.*, 1977. 73(166): 91–8.

103. Weber, W., Morris, J. Kinetics of adsorption on carbon from solution. *J. Sanit. Eng. Div.*, 1963. 89: 31–60.

104. Lagergren, S. K. About the Theory of So-called Adsorption of Soluble Substances. *Sven. Vetenskapsakad. Handingarl*, 1898. 24: 1–39.

105. Ho, Y. S., Wase, D. A. J., Forster, C. F., Forster. Removal of lead ions from aqueous solution using sphagnum moss peat as absorbent. *Water SA*, 1996. 22(3): 219–24.

106. Ritchie, A. G. Alternative to the Elovich equation for the kinetics of adsorption of gases on solids. *J. Chem. Soc. Faraday Trans. 1 Phys. Chem. Condens. Phases*, 1977. 73(3): 1650–3.

107. Guo, X., Wang, J. A general kinetic model for adsorption: Theoretical analysis and modeling. *J. Mol. Liq.*, 2019. 288: 111100.

108. Langmuir, I. The Constitution and Fundamental Properties of Solids and Liquids. Part I. Solids. *J. Am. Chem. Soc.*, 1916. 38(11): 2221–95.

109. Freundlich, H. M. Over the Adsorption in Solution. *J. Phys. Chem. A*, 1906. 57: 385–470.

110. Sips, R. On the Structure of a Catalyst Surface. *J. Chem. Phys.*, 1948. 16(5): 490–5.

111. Redlich, O., Peterson, D. L. A Useful Adsorption Isotherm. *J. Phys. Chem.*, 1959. 63(6): 1024.

112. Dubinin, M. M. The Equation of the Characteristic Curve of Activated Charcoal. *Proc. USSR Acad. Sci.*, 1947. 55: 327–9.

113. Brunauer, S., Emmett, P. H., Teller, E. Adsorption of Gases in Multimolecular Layers. *J. Am. Chem. Soc.*, 1938. 60(2): 309–19.

114. Wang, J., Guo, X. Adsorption isotherm models: Classification, physical meaning, application and solving method. *Chemosphere*, 2020. 258: 127279.

115. Kumari, P., Bahadur, N., Dumée, L. F. Photo-catalytic membrane reactors for the remediation of persistent organic pollutants – A review. *Sep. Purif. Technol.*, 2020. 230(July 2019): 115878.

116. Molinari, R., Lavorato, C., Argurio, P. Recent progress of photocatalytic membrane reactors in water treatment and in synthesis of organic compounds. A review. *Catal. Today*, 2017. 281: 144–64.

117. Leong, S., Razmjou, A., Wang, K., Hapgood, K., Zhang, X., Wang, H. TiO2 based photocatalytic membranes: A review. *J. Memb. Sci.*, 2014. 472: 167–84.

118. Chen, X., Hu, Y., Xie, Z., Wang, H. Materials and Design of Photocatalytic Membranes. Current Trends and Future Developments on (Bio-) Membranes:

Photocatalytic Membranes and Photocatalytic Membrane Reactors. Elsevier Inc.; 2018. 71–96 p.

119. Shareef, U., Othman, M. H. D., Ismail, A. F., Jilani, A. Facile removal of bisphenol A from water through novel Ag-doped TiO2 photocatalytic hollow fiber ceramic membrane. *J. Aust. Ceram. Soc.*, 2019. .

120. Luo, J., Chen, W., Song, H., Liu, J. Fabrication of hierarchical layer-by-layer membrane as the photocatalytic degradation of foulants and effective mitigation of membrane fouling for wastewater treatment. *Sci. Total Environ.*, 2020. 699: 134398.

121. Bonekamp, B. C. Preparation of asymmetric ceramic membrane supports by dip-coating. In: Burggraaf AJ, Cot LBT-MS and T, editors. Fundamentals of Inorganic Membrane Science and Technology Elsevier; 1996. p. 141–225.

122. Qu, D., Ramé, E., Garoff, S. Dip-coated films of volatile liquids. *Phys. Fluids*, 2002. 14(3): 1154–65.

123. Gutoff, E. B., Cohen, E. D. Chapter 13 - Water- and solvent-based coating technology. In: Wagner JRBT-MFP, editor. Plastics Design Library Boston: William Andrew Publishing; 2010. p. 163–84.

124. Liu, J., Chiam, S. Y., Pan, J., Wong, L. M., Li, S. F. Y., Ren, Y. Solution layer-by-layer uniform thin film dip coating of nickel hydroxide and metal incorporated nickel hydroxide and its improved electrochromic performance. *Sol. Energy Mater. Sol. Cells*, 2018. 185: 318–24.

125. Huang, Y., Sun, J., Wu, D., Feng, X. Layer-by-layer self-assembled chitosan/PAA nanofiltration membranes. *Sep. Purif. Technol.*, 2018. 207: 142–50.

126. Neacşu, I. A., Nicoară, A. I., Vasile, O. R., Vasile, B. Ş. Chapter 9 - Inorganic micro- and nanostructured implants for tissue engineering. In: Grumezescu AMBT-N in HTE, editor. William Andrew Publishing; 2016. p. 271–95.

127. Sahoo, S. K., Manoharan, B., Sivakumar, N. Introduction: Why Perovskite and Perovskite Solar Cells? In: Thomas S, Thankappan ABT-PP, editors. Perovskite Photovoltaics Elsevier; 2018. p. 1–24.

128. Pinnau, I. MEMBRANE SEPARATIONS | Membrane Preparation. In: Wilson IDBT-E of SS, editor. Encyclopedia of Separation Science Oxford: Elsevier; 2000. p. 1755–64.

129. Hu, Z., Yang, Y., Chang, Q., Liu, F., Wang, Y., Rao, J. Preparation of a High-Performance Porous Ceramic Membrane by a Two-Step Coating Method and One-Step Sintering. Vol. 9, Applied Sciences . 2018.

130. Zobel, S., Gries, T. The use of nonwovens as filtration materials. In: Chapman RABT-A of N in TT, editor. Applications of Nonwovens in Technical Textiles Elsevier; 2010. p. 160–83.

131. Rao, G., Zhang, Q., Zhao, H., Chen, J., Li, Y. Novel titanium dioxide/iron (III) oxide/graphene oxide photocatalytic membrane for enhanced humic acid removal from water. *Chem. Eng. J.*, 2016. 302: 633–40.

132. Qian, Y., Zhang, X., Liu, C., Zhou, C., Huang, A. Tuning interlayer spacing of graphene oxide membranes with enhanced desalination performance. *Desalination*, 2019. 460: 56–63.

133. Casanova, S., Liu, T.-Y., Chew, Y.-M. J., Livingston, A., Mattia, D. High flux thin-film nanocomposites with embedded boron nitride nanotubes for nanofiltration. *J. Memb. Sci.*, 2020. 597: 117749.

134. Wang, Y., Wu, N., Wang, Y., Ma, H., Zhang, J., Xu, L., Albolkany, M. K., Liu, B. Graphite phase carbon nitride based membrane for selective permeation. *Nat. Commun.*, 2019. 10(1): 2500.

135. Kuhr, M., Aibibu, D., Cherif, C. Targeted partial finishing of barrier textiles with microparticles, and their effects on barrier properties and comfort. *J. Ind. Text.*, 2014. 45(5): 853–78.

136. Gao, W., Kono, J. Science and applications of wafer-scale crystalline carbon nanotube films prepared through controlled vacuum filtration. *R. Soc. Open Sci.*, 2020. 6(3): 181605.

137. Huang, J., Hu, J., Shi, Y., Zeng, G., Cheng, W., Yu, H., Gu, Y., Shi, L., Yi, K. Evaluation of self-cleaning and photocatalytic properties of modified g-C 3 N 4 based PVDF membranes driven by visible light. *J. Colloid Interface Sci.*, 2019. 541: 356–66.

138. AlFannakh, H., Abdallah, H., Ibrahim, S. S., Souayeh, B. Low-Pressure Membrane for Water Treatment Applications. Acierno D, editor. *Int. J. Polym. Sci.*, 2020. 2020: 8893027.

139. Guillen, G. R., Pan, Y., Li, M., Hoek, E. M. V. Preparation and Characterization of Membranes Formed by Nonsolvent Induced Phase Separation: A Review. *Ind. Eng. Chem. Res.*, 2011. 50(7): 3798–817.

140. Homayoonfal, M., Mehrnia, M. R., Shariaty-Niassar, M., Akbari, A., Ismail, A. F., Matsuura, T. A comparison between blending and surface deposition methods for the preparation of iron oxide/polysulfone nanocomposite membranes. *Desalination*, 2014. 354: 125–42.

141. Li, W., Li, B., Meng, M., Cui, Y., Wu, Y., Zhang, Y., Dong, H., Feng, Y. Bimetallic Au/Ag decorated TiO2 nanocomposite membrane for enhanced photocatalytic degradation of tetracycline and bactericidal efficiency. *Appl. Surf. Sci.*, 2019. 487: 1008–17.

142. Hong, J., He, Y. Polyvinylidene fluoride ultrafiltration membrane blended with nano-ZnO particle for photo-catalysis self-cleaning. *Desalination*, 2014. 332(1): 67–75.

143. Zangeneh, H., Rahimi, Z., Zinatizadeh, A. A., Razavizadeh, S. H., Zinadini, S. l-Histidine doped-TiO2-CdS nanocomposite blended UF membranes with photocatalytic and self-cleaning properties for remediation of effluent from a local waste stabilization pond (WSP) under visible light. *Process Saf. Environ. Prot.*, 2020. 136: 92–104.

144. Hong, J., He, Y. Effects of nano sized zinc oxide on the performance of PVDF microfiltration membranes. *Desalination*, 2012. 302: 71–9.

145. Nasrollahi, N., Aber, S., Vatanpour, V., Mahmoodi, N. M. The effect of amine functionalization of CuO and ZnO nanoparticles used as additives on the morphology and the permeation properties of polyethersulfone ultrafiltration nanocomposite membranes. *Compos. Part B Eng.*, 2018. 154: 388–409.

146. Mu, Y., Zhu, K., Luan, J., Zhang, S., Zhang, C., Na, R., Yang, Y., Zhang, X., Wang, G. Fabrication of hybrid ultrafiltration membranes with improved water separation properties by incorporating environmentally friendly taurine modified hydroxyapatite nanotubes. *J. Memb. Sci.*, 2019. 577: 274–84.

147. Argurio, P., Fontananova, E., Molinari, R., Drioli, E. Photocatalytic membranes in photocatalytic membrane reactors. Vol. 6, Processes. 2018.

148. Hartig, R., Hausmann, M., Schmitt, J., Herrmann, D. B. J., Riedmiller, M., Cremer, C. Preparative continuous separation of biological particles by means of free-flow magnetophoresis in a free-flow electrophoresis chamber. *Electrophoresis*, 1992. 13(1): 674–6.

149. Winoto-Morbach, S., Tchikov, V., Müller-Ruchholtz, W. Magnetophoresis: I. detection of magnetically labeled cells. *J. Clin. Lab. Anal.*, 1994. 8(6): 400–6.

150. Suwa, M., Watarai, H. Magnetophoretic velocimetry of manganese(II) in a single emulsion droplet at the femtomole level. *Anal. Chem.*, 2001. 73(21): 5214–9.

151. Wilhelm, C., Gazeau, F., Bacri, J. C. Magnetophoresis and ferromagnetic resonance of magnetically labeled cells. *Eur. Biophys. J.*, 2002. 31(2): 118–25.

152. Lim, J. K., Yeap, S. P., Leow, C. H., Toh, P. Y., Low, S. C. Magnetophoresis of iron oxide nanoparticles at low field gradient: The role of shape anisotropy. *J. Colloid Interface Sci.*, 2014. 421: 170–7.

153. Benelmekki, M., Martinez, L. M., Andreu, J. S., Camacho, J., Faraudo, J. Magnetophoresis of colloidal particles in a dispersion of superparamagnetic nanoparticles: Theory and experiments. *Soft Matter*, 2012. 8(22): 6039–47.

154. Pethig, R. Review Article—Dielectrophoresis: Status of the theory, technology, and applications. *Biomicrofluidics*, 2010. 4(022811): 1–29.

155. Todd, P., Plank, L. D., Kunze, M. E., Lewis, M. L., Morrison, D. R., Barlow, G. H., Lanham, J. W., Cleveland, C., Astronautics, M. Electrophoretic separation and analysis of living cells from solid tissues by several methods. Human embryonic kidney cell cultures as a model. *J. Chromatogr.*, 1986. 364: 11–24.

156. Liang, L. Particle Electrophoresis and Magnetophoresis in Microchannels. Clemson University; 2013.

157. Jones, T. Dielectrophoresis and magnetophoresis. In: Press CU, editor. Electromechanics of Particles 1st ed. New York: Cambridge University Press; 1995. p. 34–82.

158. Munaz, A., Shiddiky, M. J. A., Nguyen, N. T. Recent advances and current challenges in magnetophoresis based micro magnetofluidics. *Biomicrofluidics*, 2018. 12(3): 24.

159. Whitesides, G. M. The origins and the future of microfluidics. *Nature*, 2006. 442: 368.

160. Hejazian, M., Li, W., Nguyen, N. T. Lab on a chip for continuous-flow magnetic cell separation. *Lab Chip*, 2015. 15(4): 959–70.

161. Pamme, N. Magnetism and microfluidics. *Lab Chip*, 2006. 6(1): 24–38.

162. Nguyen, N. T. Micro-magnetofluidics: Interactions between magnetism and fluid flow on the microscale. *Microfluid. Nanofluidics*, 2012. 12(1–4): 1–16.

163. Safarík, I., Safaríková, M. Use of magnetic techniques for the isolation of cells. *J. Chromatogr. B Biomed. Sci. Appl.*, 1999. 722(1–2): 33–53.

164. Nilsson, J., Evander, M., Hammarström, B., Laurell, T. Review of cell and particle trapping in microfluidic systems. *Anal. Chim. Acta*, 2009. 649(2): 141–57.

165. Cornell, R. M., Schwertmann, U. Introduction to the Iron Oxides. In: The Iron Oxides: Structure, Properties, Reactions, Occurrences and Uses 2nd ed. Weinheim: Wiley-VCH Verlag GmbH & Co.; 2006. p. 705.

166. Zhang, X., Fang, X., Li, J., Pan, S., Sun, X., Shen, J., Han, W., Wang, L., Zhao, S. Developing new adsorptive membrane by modification of support layer with iron oxide microspheres for arsenic removal. *J. Colloid Interface Sci.*, 2018. 514: 760–8.

167. Hoshi, Y., Naoe, M. Crystalline Orientation and Perpendicular Magnetic Anisotropy of Iron Oxide Thin Films Deposited by Target Facing Type Sputtering. *IEEE Transl. J. Magn. Japan*, 1987. 2(5): 431–3.

168. Bruno, P. Tight-binding approach to the orbital magnetic moment and magnetocrystalline anisotropy of transition-metal monolayers. *Phys. Rev. B*, 1989. 39(1): 865–8.

169. Daraei, P., Madaeni, S. S., Ghaemi, N., Khadivi, M. A., Astinchap, B., Moradian, R. Fouling resistant mixed matrix polyethersulfone membranes blended with magnetic nanoparticles: Study of magnetic field induced casting. *Sep. Purif. Technol.*, 2013. 109: 111–21.

170. Huang, Z., Zheng, F., Zhang, Z., Xu, H., Zhou, K. The performance of the PVDF-Fe3O4 ultrafiltration membrane and the effect of a parallel magnetic field used during the membrane formation. *Desalination*, 2012. 292: 64–72.

171. Huang, Y., Xiao, C. fa., Huang, Q. lin., Liu, H. liang., Hao, J. qiang., Song, L. Magnetic field induced orderly arrangement of Fe3O4/GO composite particles for preparation of Fe3O4/GO/PVDF membrane. *J. Memb. Sci.*, 2018. 548(399): 184–93.

172. Nor, N. A. M., Jaafar, J., Ismail, A. F., Mohamed, M. A., Rahman, M. A., Othman, M. H. D., Lau, W. J., Yusof, N. Preparation and performance of PVDF-based nanocomposite membrane consisting of TiO2 nanofibers for organic pollutant decomposition in wastewater under UV irradiation. *Desalination*, 2016. 391: 89–97.

173. Mohamed, M. A., W. Salleh, W. N., Jaafar, J., Ismail, A. F., Mutalib, M. A., Sani, N. A. A., M. Asri, S. E. A., Ong, C. S. Physicochemical characteristic of regenerated cellulose/N-doped TiO2 nanocomposite membrane fabricated from recycled newspaper with photocatalytic activity under UV and visible light irradiation. *Chem. Eng. J.*, 2016. 284: 202–15.

174. Yeoh, G. H., Tu, J. Liquid–Particle Flows. In: Yeoh GH, Tu JBT-CT for MF, editors. Computational Techniques for Multiphase Flows Oxford: Elsevier; 2010. p. 313–49.

175. Xu, Z. M. B. of M. G. O. via M. F. I. C. and P. S. toward H.-P. H. U. M., Wu, T., Shi, J., Wang, W., Teng, K., Qian, X., Shan, M., Deng, H., Tian, X., Li, C., Li, F. Manipulating Migration Behavior of Magnetic Graphene Oxide via Magnetic Field Induced Casting and Phase Separation toward High-Performance Hybrid Ultrafiltration Membranes. *ACS Appl. Mater. Interfaces*, 2016. 8(28): 18418–29.

176. Rastgar, M., Shakeri, A., Bozorg, A., Salehi, H., Saadattalab, V. Highly-efficient forward osmosis membrane tailored by magnetically responsive graphene oxide/Fe3O4 nanohybrid. *Appl. Surf. Sci.*, 2018. 441: 923–35.

177. Ma, J., Liu, C., Chen, K. Counting on low-oxygen calcination to boost zinc ferrite powder's topology and photocatalytic efficiency. *Adv. Powder Technol.*, 2020. 31(4): 1372–80.

178. Gholami, M., Zare-Hoseinabadi, A., Mohammadi, M., Taghizadeh, S., Behbahani, A. B., Amani, A. M., Solghar, R. A. Preparation of ZnXFe3-XO4@chitosan nanoparticles as an adsorbent for methyl orange and phenol. *J. Environ. Treat. Tech.*, 2019. 7(3): 245–9.

179. Ignat, M., Samoila, P., Cojocaru, C., Sacarescu, L., Harabagiu, V. Novel Synthesis Route for Chitosan-Coated Zinc Ferrite Nanoparticles as Potential Sorbents for Wastewater Treatment. *Chem. Eng. Commun.*, 2016. 203(12): 1591–9.

180. Patnaik, S., Das, K. K., Mohanty, A., Parida, K. Enhanced photo catalytic reduction of Cr (VI) over polymer-sensitized g-C3N4/ZnFe2O4 and its synergism with phenol oxidation under visible light irradiation. *Catal. Today*, 2018. 315(November 2017): 52–66.

181. Yanagida, S., Kosakai, Y., Yasumori, A. Preparation of gold nanoparticle dispersed TiO2-polymer composite film by a combined layer-by-layer and

photocatalytic deposition method. *Colloids Surfaces A Physicochem. Eng. Asp.*, 2014. 456(1): 55–61.

182. Dong, G., Li, H., Chen, V. Challenges and opportunities for mixed-matrix membranes for gas separation. *J. Mater. Chem. A*, 2013. 1(15): 4610–30.

183. Khayet, M., Suk, D. E., Narbaitz, R. M., Santerre, J. P., Matsuura, T. Study on surface modification by surface-modifying macromolecules and its applications in membrane-separation processes. *J. Appl. Polym. Sci.*, 2003. 89(11): 2902–16.

184. Salim, N. E., Jaafar, J., Ismail, A. F., Othman, M. H. D., Rahman, M. A., Yusof, N., Qtaishat, M., Matsuura, T., Aziz, F., Salleh, W. N. W. Preparation and characterization of hydrophilic surface modifier macromolecule modified poly (ether sulfone) photocatalytic membrane for phenol removal. *Chem. Eng. J.*, 2018. 335(October): 236–47.

185. Mohd Norddin, M. N. A., Ismail, A. F., Rana, D., Matsuura, T., Mustafa, A., Tabe-Mohammadi, A. Characterization and performance of proton exchange membranes for direct methanol fuel cell: Blending of sulfonated poly(ether ether ketone) with charged surface modifying macromolecule. *J. Memb. Sci.*, 2008. 323(2): 404–13.

186. Liu, S., Li, D., Sun, H., Ang, H. M., Tadé, M. O., Wang, S. Oxygen functional groups in graphitic carbon nitride for enhanced photocatalysis. *J. Colloid Interface Sci.*, 2016. 468: 176–82.

187. Sahebi, S., Phuntsho, S., Woo, Y. C., Park, M. J., Tijing, L. D., Hong, S., Shon, H. K. Effect of sulphonated polyethersulfone substrate for thin film composite forward osmosis membrane. *Desalination*, 2016. 389: 129–36.

188. Rana, D., Matsuura, T., Narbaitz, R. M. Novel hydrophilic surface modifying macromolecules for polymeric membranes: Polyurethane ends capped by hydroxy group. *J. Memb. Sci.*, 2006. 282(1): 205–16.

189. Tang, R., Ding, R., Xie, X. Preparation of oxygen-doped graphitic carbon nitride and its visible-light photocatalytic performance on bisphenol A degradation. *Water Sci. Technol.*, 2018. 78(5): 1023–33.

190. Moslehyani, A., Ismail, A. F., Othman, M. H. D., Matsuura, T. Design and performance study of hybrid photocatalytic reactor-PVDF/MWCNT nanocomposite membrane system for treatment of petroleum refinery wastewater. *Desalination*, 2015. 363: 99–111.

191. Scherrer, P. Nachr Ges Wiss Goettingen. *Math. Phys.*, 1918. 2: 98–100.

192. Rani, N., Chahal, S., Chauhan, A. S., Kumar, P., Shukla, R., Singh, S. K. X-ray Analysis of MgO Nanoparticles by Modified Scherer's Williamson-Hall and Size-Strain Method. *Mater. Today Proc.*, 2019. 12: 543–8.

193. Mote, V., Purushotham, Y., Dole, B. Williamson-Hall analysis in estimation of lattice strain in nanometer-sized ZnO particles. *J. Theor. Appl. Phys.*, 2012. 6(1): 2–9.

194. Williamson, G. K., Hall, W. H. X-ray line broadening from filed aluminium and wolfram. *Acta Metall.*, 1953. 1(1): 22–31.

195. Bragg, W. L. H., Bragg, W. L. H. The structure of some crystals as indicated by their diffraction of X-rays. *Proc. R. Soc. London. Ser. A, Contain. Pap. a Math. Phys. Character*, 1913. 89(610): 248–77.

196. Yuan, W., Yuan, P., Liu, D., Yu, W., Deng, L., Chen, F. Novel hierarchically porous nanocomposites of diatomite-based ceramic monoliths coated with silicalite-1 nanoparticles for benzene adsorption. *Microporous Mesoporous Mater.*, 2015. 206(C): 184–93.

197. Shukla, A. K., Alam, J., Alhoshan, M., Dass, L. A., Muthumareeswaran, M. R. Development of a nanocomposite ultrafiltration membrane based on polyphenylsulfone blended with graphene oxide. *Sci. Rep.*, 2017. 7(October 2016): 1–12.

198. Thiele, G., Poston, M., Brown, R. A case study sizing Nanoparticles. *234th ACS Natl. Meet.*, 2007. : 316.

199. Deville, J.-P., Cojocaru, C. S. Chapter 12 - Spectroscopic Analyses of Surfaces and Thin Films. In: Pauleau YBT-MSP by DET, editor. European Materials Research Society Series Oxford: Elsevier; 2006. p. 411–41.

200. Raeisi Shahraki, R., Ebrahimi, M., Seyyed Ebrahimi, S. A., Masoudpanah, S. M. Structural characterization and magnetic properties of superparamagnetic zinc ferrite nanoparticles synthesized by the coprecipitation method. *J. Magn. Magn. Mater.*, 2012. 324(22): 3762–5.

201. Holzwarth, U., Gibson, N. The Scherrer equation versus the "Debye-Scherrer equation." Vol. 6, Nature Nanotechnology. 2011. p. 534.

202. Kose, A., Ozaki, M., Takano, K., Kobayashi, Y., Hachisu, S. Direct observation of ordered latex suspension by metallurgical microscope. *J. Colloid Interface Sci.*, 1973. 44(2): 330–8.

203. Agbaje, T. A., Al-Gharabli, S., Mavukkandy, M. O., Kujawa, J., Arafat, H. A. PVDF/magnetite blend membranes for enhanced flux and salt rejection in membrane distillation. *Desalination*, 2018. 436(January): 69–80.

204. Patil, R. P., Delekar, S. D., Mane, D. R., Hankare, P. P. Synthesis, structural and magnetic properties of different metal ion substituted nanocrystalline zinc ferrite. *Results Phys.*, 2013. 3(3): 129–33.

205. Waldron, R. D. Infrared Spectra of Ferrites. *Phys. Rev.*, 1955. 99(6): 1727–35.

206. Coey, J. M. D. Magnetism and Magnetic Materials. Cambridge: Cambridge University Press; 2010.

207. Szczerba, W., Zukrowski, J., Przybylski, M., Sikora, M., Safonova, O., Shmeliov, A., Nicolosi, V., Schneider, M., Granath, T., Oppmann, M., Straßer, M., Mandel, K. Pushing up the magnetisation values for iron oxide nanoparticles: Via zinc doping: X-ray studies on the particle's sub-nano structure of different synthesis routes. *Phys. Chem. Chem. Phys.*, 2016. 18(36): 25221–9.

208. Widhyahrini, K., Handayani, N., Wahyuningrum, D., Radiman, C. L. The synthesis of sulfonated polyethersulfone (SPES) and the preparation of its membranes as matrix in the immobilization of Candida antarctica lipase B (Cal-B). *Polym. Bull.*, 2020. 77(7): 3735–48.

209. Belfer, S., Fainchtain, R., Purinson, Y., Kedem, O. Surface characterization by FTIR-ATR spectroscopy of polyethersulfone membranes-unmodified, modified and protein fouled. *J. Memb. Sci.*, 2000. 172(1): 113–24.

210. Abdul Mannan, H., Mukhtar, H., Shima Shaharun, M., Roslee Othman, M., Murugesan, T. Polysulfone/poly(ether sulfone) blended membranes for CO2 separation. *J. Appl. Polym. Sci.*, 2016. 133(5): 1–9.

211. Alayande, A. B., Obaid, M., Yu, H. W., Kim, I. S. High-flux ultrafiltration membrane with open porous hydrophilic structure using dual pore formers. *Chemosphere*, 2019. 227: 662–9.

212. Ghanbarian, B., Hunt, A. G., Ewing, R. P., Sahimi, M. Tortuosity in Porous Media: A Critical Review. *Soil Sci. Soc. Am. J.*, 2013. 77(5): 1461–77.

213. Adler, P. M. Porous Media: Geometry and Transports. Butterworth-Heinemann; 1992. (Butterworth-Heinemann series in chemical engineering).

214. Zhang, J. Interfacial Energy. In: Wang QJ, Chung Y-W, editors. Encyclopedia of Tribology Boston, MA: Springer US; 2013. p. 1840–1840.

215. Azizian, S. Kinetic models of sorption: A theoretical analysis. *J. Colloid Interface Sci.*, 2004. 276(1): 47–52.

216. Adamczyk, Z., Siwek, B., Zembala, M. Reversible and irreversible adsorption of particles on homogeneous surfaces. *Colloids and Surfaces*, 1992. 62(1–2): 119–30.

217. Lorenc-Grabowska, E. Effect of micropore size distribution on phenol adsorption on steam activated carbons. *Adsorption*, 2016. 22(4–6): 599–607.

218. Schaaf, P., Talbot, J. Surface exclusion effects in adsorption processes. *J. Chem. Phys.*, 1989. 91(7): 4401–9.

219. dos Santos, J. M. N., Pereira, C. R., Foletto, E. L., Dotto, G. L. Alternative synthesis for ZnFe2O4 /chitosan magnetic particles to remove diclofenac from water by adsorption. *Int. J. Biol. Macromol.*, 2019. 131: 301–8.

220. Aerts, P., Van Hoof, E., Leysen, R., Vankelecom, I. F. ., Jacobs, P. . Polysulfone–Aerosil composite membranes Part 1. The influence of the addition of Aerosil on the formation process and membrane morphology. *J. Memb. Sci.*, 2000. 176(1): 63–73.

221. Sadrzadeh, M., Bhattacharjee, S. Rational design of phase inversion membranes by tailoring thermodynamics and kinetics of casting solution using polymer additives. *J. Memb. Sci.*, 2013. 441: 31–44.

222. Somvanshi, S. B., Kharat, P. B., Khedkar, M. V., Jadhav, K. M. Hydrophobic to hydrophilic surface transformation of nano-scale zinc ferrite via oleic acid coating: Magnetic hyperthermia study towards biomedical applications. *Ceram. Int.*, 2020. 46(6): 7642–53.

223. Maximous, N., Nakhla, G., Wan, W., Wong, K. Effect of the metal oxide particle distributions on modified PES membranes characteristics and performance. *J. Memb. Sci.*, 2010. 361(1–2): 213–22.

224. Crank, J. The mathematics of diffusion. Oxford university press; 1979.

225. Tseng, R. L., Wu, F. C., Juang, R. S. Characteristics and applications of the Lagergren's first-order equation for adsorption kinetics. *J. Taiwan Inst. Chem. Eng.*, 2010. 41(6): 661–9.

226. Zhang, J. Physical insights into kinetic models of adsorption. *Sep. Purif Technol.*, 2019. 229(July): 115832.

227. Eris, S., Azizian, S. Analysis of adsorption kinetics at solid/solution interface using a hyperbolic tangent model. *J. Mol. Liq.*, 2017. 231: 523–7.

228. Rudzinski, W., Plazinski, W. Studies of the kinetics of solute adsorption at solid/solution interfaces: On the possibility of distinguishing between the diffusional and the surface reaction kinetic models by studying the pseudo-first-order kinetics. *J. Phys. Chem. C*, 2007. 111(41): 15100–10.

229. Vogrin, N., Stropnik, Č., Musil, V., Brumen, M. The wet phase separation: The effect of cast solution thickness on the appearance of macrovoids in the membrane forming ternary cellulose acetate/acetone/water system. *J. Memb. Sci.*, 2002. 207(1): 139–41.

230. Cheung, C. W., Porter, J. F., Mckay, G. Sorption kinetic analysis for the removal of cadmium ions from effluents using bone char. *Water Res.*, 2001. 35(3): 605–12.

231. Weber, T. W., Chakravorti, R. K. Pore and solid diffusion models for fixed-bed adsorbers. *AIChE J.*, 1974. 20(2): 228–38.

232. Mojoudi, N., Mirghaffari, N., Soleimani, M., Shariatmadari, H., Belver, C., Bedia, J. Phenol adsorption on high microporous activated carbons prepared from oily sludge: equilibrium, kinetic and thermodynamic studies. *Sci. Rep.*, 2019. 9(1): 1–12.

233. Rowley, J., Abu-Zahra, N. H. Synthesis and characterization of polyethersulfone membranes impregnated with (3-aminopropyltriethoxysilane) APTES-Fe3O4 nanoparticles for As(V) removal from water. *J. Environ. Chem. Eng.*, 2019. 7(1): 102875.

234. Ghafari, M., Cui, Y., Alali, A., Atkinson, J. D. Phenol adsorption and desorption with physically and chemically tailored porous polymers: Mechanistic variability associated with hyper-cross-linking and amination. *J. Hazard. Mater.*, 2019. 361: 162–8.

235. Kow, S.-H., Fahmi, M. R., Abidin, C. Z. A., Ong, S.-A., Ibrahim, N. Regeneration of spent activated carbon from industrial application by NaOH solution and hot water. *Desalin. Water Treat.*, 2016. 57(60): 29137–42.

236. Nambikkattu, J., Kaleekkal, N. J., Jacob, J. P. Metal ferrite incorporated polysulfone thin-film nanocomposite membranes for wastewater treatment. *Environ. Sci. Pollut. Res.*, 2020. .

237. Guillen, G. R., Ramon, G. Z., Kavehpour, H. P., Kaner, R. B., Hoek, E. M. V. Direct microscopic observation of membrane formation by nonsolvent induced phase separation. *J. Memb. Sci.*, 2013. 431: 212–20.

238. Young, T. H., Chen, L. W. Pore formation mechanism of membranes from phase inversion process. *Desalination*, 1995. 103(3): 233–47.

239. Ren, J., Li, Z., Wong, F.-S. Membrane structure control of BTDA-TDI/MDI (P84) co-polyimide asymmetric membranes by wet-phase inversion process. *J. Memb. Sci.*, 2004. 241(2): 305–14.

240. Feng, Y., Han, G., Chung, T. S., Weber, M., Widjojo, N., Maletzko, C. Effects of polyethylene glycol on membrane formation and properties of hydrophilic sulfonated polyphenylenesulfone (sPPSU) membranes. *J. Memb. Sci.*, 2017. 531(February): 27–35.

241. Lee, C.-G. Calculation of light penetration depth in photobioreactors. *Biotechnol. Bioprocess Eng.*, 1999. 4(1): 78–81.

242. Goetzberger, A., Knobloch, J., Voß, B. The Physics of Solar Cells. Crystalline Silicon Solar Cells. 2014. p. 67–86.

243. Solvay. Optical Properties of Sulfone Polymers. Solvay; 2014. p. 3.

244. Onyango, M. S., Kojima, Y., Aoyi, O., Bernardo, E. C., Matsuda, H. Adsorption equilibrium modeling and solution chemistry dependence of fluoride removal from water by trivalent-cation-exchanged zeolite F-9. *J. Colloid Interface Sci.*, 2004. 279(2): 341–50.

245. Hutson, N. D., Yang, R. T. Theoretical basis for the Dubinin-Radushkevitch (D-R) adsorption isotherm equation. *Adsorption*, 1997. 3(3): 189–95.

246. Brunauer, S., Emmett, P. H. The Use of Low Temperature van der Waals Adsorption Isotherms in Determining the Surface Areas of Various Adsorbents. *J. Am. Chem. Soc.*, 1937. 59(12): 2682–9.

247. Jeyachandran, Y. L., Mielczarski, E., Rai, B., Mielczarski, J. A. Quantitative and qualitative evaluation of adsorption/desorption of bovine serum albumin on hydrophilic and hydrophobic surfaces. *Langmuir*, 2009. 25(19): 11614–20.

248. Zhang, M., Song, L. Mechanisms and Parameters Affecting Flux Decline in Cross-Flow Microfiltration and Ultrafiltration of Colloids. *Environ. Sci. Technol.*, 2000. 34(17): 3767–73.

249. Piry, A., Heino, A., Kühnl, W., Grein, T., Ripperger, S., Kulozik, U. Effect of membrane length, membrane resistance, and filtration conditions on the fractionation of milk proteins by microfiltration. *J. Dairy Sci.*, 2012. 95(4): 1590–602.

250. Srebnik, S. Polymer adsorption on multicomponent surfaces with relevance to membrane fouling. *Chem. Eng. Sci.*, 2003. 58(23): 5291–8.

251. Ho, Y. S., McKay, G. Pseudo-second order model for sorption processes. *Process Biochem.*, 1999. 34(5): 451–65.

252. Brill, T. B., Falk, D. S. Light: Its interaction with art and antiquities. *Am. J. Phys.*, 1981. 49(5): 510.

LIST OF PUBLICATIONS

1. Said KAM, Ismail AF, Zulhairun AK, Abdullah MS, Azali MA, Hafeez A. Relationship of Magnetic Strength to Zinc Ferrite Migration in Fabricating Photocatalytic Membrane for Phenol Photodegradation. J Environ Chem Eng. 2021;9(5):105923.

2. Mohamad Said KA, Ismail AF, Zulhairun AK, Abdullah MS, Usman J, Azali MA, et al. Zinc ferrite migration dependence on magnetic induce membrane for phenol removal: Adsorption reaction and diffusion study. J Environ Chem Eng. 2021;9(1):105036.

3. Mohamad Said KA, Ismail AF, Karim ZA, Abdullah MS, Hafeez A, Azali MA. Magnetic rod induced asymmetric membrane: Effect of iron oxide composition to phenol removal by adsorption. Mater Chem Phys. 2021;258(April 2020):123862.

4. Mohamad Said KA, Ismail AF, Abdul Karim Z, Abdullah MS, Hafeez A. A review of technologies for the phenolic compounds recovery and phenol removal from wastewater. Process Saf Environ Prot. 2021;151:257–89.

5. Mohamad Said KA, Ismail AF, Karim ZA, Abdullah MS, Usman J, Raji YO. Innovation in membrane fabrication: Magnetic induced photocatalytic membrane. J Taiwan Inst Chem Eng. 2020;113:372–95.

6. Mohamad Said, K. A., Ismail, A. F., Zulhairun, A. K., Abdullah, M. S., Azali, M. A., Zainal Abidin, M. N. Magnetic induced asymmetric membrane: Effect of magnetic pattern to phenol removal by adsorption. Mater. Chem. Phys., 2022; 278(August 2021): 125692.

7. Usman J, Othman MHD, Ismail AF, Rahman MA, Jaafar J, Raji YO, Mohamad Said KA et al. An overview of superhydrophobic ceramic membrane surface modification for oil-water separation. J Mater Res Technol. 2021 Mar;108947.

8. Raji YO, Othman MHD, Sapiaa Md Nordin NAH, Adam MR, Mohd Said KA, Ismail AF, et al. Synthesis and characterization of superoleophobic fumed alumina nanocomposite coated via the sol-gel process onto ceramic-based hollow fibre membrane for oil-water separation. Ceram Int. 2021;47(18):25883–94.

9. Hafeez A, Karim ZA, Ismail AF, Samavati A, Said KAM, Selambakkannu S. Functionalized boron nitride composite ultrafiltration membrane for dye removal from aqueous solution. J Memb Sci. 2020 Oct;612(June):118473.

10. Raji YO, Othman MHD, Nordin NAHSM, Adam MR, Said KAM, Abdulyekeen KA, et al. Optimization of a High-Performance Poly(diallyl dimethylammonium chloride)-alumina-perfluorooctanoate Intercalated

Ultrafiltration Membrane for Treating Emulsified Oily Wastewater via Response Surface Methodology Approach. Membranes (Basel). 2021 Dec 1;11(12):956.